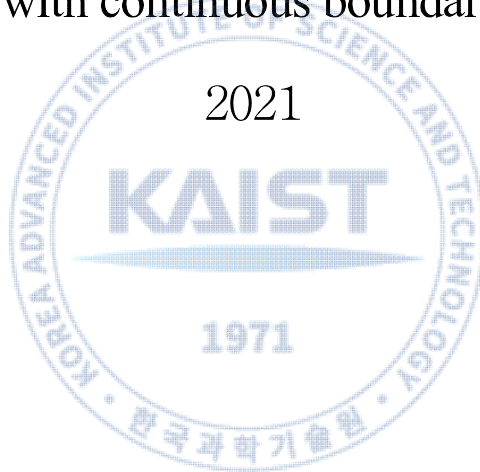


석사 학위논문  
Master's Thesis

연속적인 경계를 가지는  
절점밀도 기반 위상 최적화

A nodal density based topology optimization  
with continuous boundary

2021



이 진 환 (李 辰 煥 Lee, Jinhwan)

한 국 과 학 기 술 원

Korea Advanced Institute of Science and Technology

석사 학위논문

연속적인 경계를 가지는  
절점밀도 기반 위상 최적화

2021



이 진 환

한 국 과 학 기 술 원

기계항공공학부/기계공학과

# 연속적인 경계를 가지는 절점밀도 기반 위상 최적화

이 진 환

위 논문은 한국과학기술원 석사학위논문으로  
학위논문 심사위원회의 심사를 통과하였음

KAIST

2020년 12월 22일

심사위원장 이 필 승

심 사 위 원 이 익 진

심 사 위 원 장 인 권



# A nodal density based topology optimization with continuous boundary

Lee, Jinhwan

Advisor: Phill-Seung Lee

A thesis submitted to the faculty of  
Korea Advanced Institute of Science and Technology in  
partial fulfillment of the requirements for the degree of  
Master of Science in Mechanical Engineering

**KAIST**  
Daejeon, Korea

December 22, 2020

Approved by

  
Phill-Seung Lee

Professor of Mechanical Engineering

The study was conducted in accordance with Code of Research Ethics<sup>1)</sup>.

---

1) Declaration of Ethical Conduct in Research: I, as a graduate student of Korea Advanced Institute of Science and Technology, hereby declare that I have not committed any act that may damage the credibility of my research. This includes, but is not limited to, falsification, thesis written by someone else, distortion of research findings, and plagiarism. I confirm that my dissertation contains honest conclusions based on my own careful research under the guidance of my advisor.



MME

이진환. 연속적인 경계를 가지는 절점밀도 기반 위상 최적화. 기계공학과. 2021년. 53+v쪽. 지도교수: 이필승. (영문 논문)

Lee, Jinhwan. A nodal density based topology optimization with continuous boundary. Department of Mechanical Engineering. 2021. 54+v pages. Advisor: Lee, Phill-Seung. (Text in English)

### 초 록

위상 최적화는 구조 최적화 방법론 중 하나로써, 개념설계 단계에 주로 쓰이는 방법론이다. 본 학위 논문에서는 밀도법 기반의 위상 최적화의 경계 표현을 향상하기 위해 요소의 절점에 설계 변수를 두고 새로운 강성 식을 제안한다. 기존 요소 기반 밀도에서는 요소 내에서 항상 일정한 밀도를 가지는 특성 때문에, 경계 표현에 한계가 있다. 요소 기반 밀도법은 요소 세분화를 통해 부드러운 경계 조건을 얻을 수 있다. 본 기법에서는 각 절점이 밀도값을 가지고 임계 밀도에서 등 밀도선으로 요소를 구분하기 위해서 선형 보간된다. 제안된 강성 식은 민감도 해석에서 변형에너지를 이용해 안정적인 수렴을 할 수 있도록 한다. 위상 최적화에서 여러 수치 예제를 통해서 제안된 방법론의 검증이 수행되었다.

핵심낱말 구조 최적화, 위상 최적화, 등 밀도선, 연속적인 경계, 구조해석

### Abstract

Topology optimization is one of the structural optimization methodologies, which has been widely used in the conceptual design stage. In this thesis, in order to improve the boundary representation of the density based topology optimization, a new stiffness matrix is proposed by placing design variables at the nodes of the element. In the existing element density method, there is a limit to the boundary expression because of the characteristic that the density is constant in an element. Element density based method could provide smooth boundary with mesh refinement.

In this proposed methodology, each node has density values which are linearly interpolated to divide the element at the threshold density by an iso-density line. The proposed stiffness matrix enables stable convergence using strain energy in sensitivity analysis. Verification of the proposed methodology was performed through several numerical examples in topology optimization.

Keywords structural optimization, topology optimization, iso-density line, continuous boundary, structural analysis

## Contents

Contents.....	i
List of Tables.....	iii
List of Figures.....	iv
Chapter 1. Introduction.....	1
Chapter 2. Research background.....	3
2.1. Structural optimization.....	3
2.2. Topology optimization method .....	4
2.2.1. Homogenization method .....	4
2.2.2. ESO (Evolutionary Structural Optimization) method .....	4
2.2.3. Level set method.....	5
2.2.4. SIMP (Solid Isotropic Material with Penalization) method.....	5
2.3. Topology optimization formulation.....	6
2.3.1 Minimum compliance problem .....	6
2.3.2 Mathematical formulation for the minimum compliance problem .....	6
2.4. Optimizer for topology optimization.....	8
2.4.1. Optimality criteria method .....	8
2.4.2. The method of moving asymptotes .....	8
2.5. Filtering scheme.....	10
2.5.1 Sensitivity filter.....	10
2.5.2 Density filter .....	11
2.5.3. Heaviside projection filter.....	12
2.5.4. Alternative sensitivity filter .....	13
2.6. Introduction of iso-density line.....	14
2.7. Numerical integration scheme .....	16
2.7.1. Triangle domain.....	16
2.7.2. Quadrilateral domain .....	17
2.7.3. Other domains .....	18
Chapter 3. Nodal density based topology optimization .....	20
3.1. Formulation of proposed method for minimum compliance.....	20
3.2. Sensitivity Analysis.....	22
3.2.1. Derivatives of stiffness matrix for triangle domain.....	24
3.2.2. Derivatives of stiffness matrix for quadrilateral domain .....	24
3.2.3. Derivatives of stiffness matrix for pentagon domain .....	25
3.2.4. Derivatives of stiffness matrix for two triangles domain .....	26
3.2.5. Derivatives of stiffness matrix for hexagon domain .....	26
3.3. Optimization Procedure.....	29
Chapter 4. Numerical example.....	30
4.1. MBB beam problem .....	30

4.2. Cantilever beam problem.....	34
4.3. Michell type structure problem .....	36
Chapter 5. Conclusions.....	51
Bibliography .....	52



## List of Tables

Table 4.1. MBB problem comparison for $60 \times 20$ elements.....	32
Table 4.2. MBB problem comparison for $90 \times 30$ elements.....	32
Table 4.3. MBB problem comparison for $120 \times 40$ elements.....	33
Table 4.4. MBB problem comparison for $180 \times 60$ elements.....	33
Table 4.5. Cantilever problem comparison for $60 \times 30$ elements.....	34
Table 4.6. Cantilever problem comparison for $80 \times 40$ elements.....	35
Table 4.7. Cantilever problem comparison for $100 \times 50$ elements.....	35
Table 4.8. Cantilever problem comparison for $120 \times 60$ elements.....	35
Table 4.9. Michell type structure problem comparison for $60 \times 30$ elements.....	36
Table 4.10. Michell type structure problem comparison for $80 \times 40$ elements.....	37
Table 4.11. Michell type structure problem comparison for $100 \times 50$ elements.....	37
Table 4.12. Michell type structure problem comparison for $120 \times 60$ elements.....	37



## List of Figures

Fig. 2.1 Projection scheme within filter radius from element e.....	13
Fig. 2.2 Linear projection scheme weight function .....	13
Fig. 2.3 Implementation of iso-density line .....	14
Fig. 2.4 Iso-density line case in marching square algorithm.....	15
Fig. 2.5 Ambiguous case in marching square algorithm.....	15
Fig. 2.6 Typical case of divided domain.....	16
Fig. 2.7 Summation of domain for stiffness calculation .....	19
Fig. 3.1 Case of domain set.....	21
Fig. 3.2 Case for location of node .....	22
Fig. 3.3 Triangle domain.....	27
Fig. 3.4 Quadrilateral domain .....	27
Fig. 3.5 Pentagon domain .....	28
Fig. 3.6 Two triangles domain.....	28
Fig. 3.7 Hexagon domain .....	28
Fig. 3.8 Procedure of topology optimization.....	29
Fig. 4.1. MBB beam problem .....	30
Fig. 4.2. Initial design for optimization .....	30
Fig. 4.3 Measure of discreteness of both method.....	31
Fig. 4.4. Cantilever beam problem.....	34
Fig. 4.5. Michell type structure problem.....	36
Fig. 4.6. 60×20 MBB beam problem Proposed method (top) and SIMP method (bottom).....	39
Fig. 4.7. Iterative process of 60×20 elements.....	39
Fig. 4.8. Optimization results for 60×20 elements.....	39
Fig. 4.9. 90×30 MBB beam problem Proposed method (top) and SIMP method (bottom).....	40
Fig. 4.10. Iterative process of 90×30 elements.....	40
Fig. 4.11. Optimization results for 90×30 elements.....	40
Fig. 4.12. 120×40 MBB beam problem proposed method (top) and SIMP method (bottom) .....	41
Fig. 4.13. Iterative process of 120×40 elements.....	41
Fig. 4.14. Optimization results for 120×40 elements.....	41
Fig. 4.15. 180×60 MBB beam problem proposed method (top) and SIMP method (bottom) .....	42
Fig. 4.16. Iterative process of 180×60 elements.....	42
Fig. 4.17. Optimization results for 180×60 elements.....	42
Fig. 4.18. 60×30 Cantilever beam problem proposed method (top) and SIMP method (bottom).....	43
Fig. 4.19. Iterative process of 60×30 elements.....	43
Fig. 4.20. Optimization results for 60×30 elements.....	43
Fig. 4.21. 80×40 Cantilever beam problem proposed method (top) and SIMP method (bottom).....	44
Fig. 4.22. Iterative process of 80×40 elements.....	44

Fig. 4.23. Optimization results for 80×40 elements.....	44
Fig. 4.24. 100×50 Cantilever beam problem proposed method (top) and SIMP method (bottom) .....	45
Fig. 4.25. Iterative process of 100×50 elements .....	45
Fig. 4.26. Optimization results for 100×50 elements.....	45
Fig. 4.27. 120×60 Cantilever beam problem proposed method (top) and SIMP method (bottom) .....	46
Fig. 4.28. Iterative process of 120×60 elements .....	46
Fig. 4.29. Optimization results for 120×60 elements.....	46
Fig. 4.30. 60×30 Michell type structure problem proposed method (top) and SIMP method (bottom).....	47
Fig. 4.31. Iterative process of 60×30 elements.....	47
Fig. 4.32. Optimization results for 60×30 elements .....	47
Fig. 4.33. 80×40 Michell type structure problem proposed method (top) and SIMP method (bottom).....	48
Fig. 4.34. Iterative process of 80×40 elements.....	48
Fig. 4.35. Optimization results for 80×40 elements.....	48
Fig. 4.36. 100×50 Michell type structure problem proposed method (top) and SIMP method (bottom) .....	49
Fig. 4.37. Iterative process of 100×50 elements .....	49
Fig. 4.38. Optimization results for 100×50 elements.....	49
Fig. 4.39. 120×60 Michell type structure problem proposed method (top) and SIMP method (bottom) .....	50
Fig. 4.40. Iterative process of 120×60 elements.....	50
Fig. 4.41. Optimization results for 120×60 elements.....	50

## Chapter 1. Introduction

Topology optimization is one of the structural optimization methodologies that suggest how to place materials to obtain the most optimal performance. This has gained popularity over the past decades and has been applied in various fields such as fluid, acoustics, and metamaterial design as well as structural optimization. In addition, various topological optimization design techniques have been developed, and actual manufacturable design techniques have been considered with the development of additive manufacturing. When considering manufacturability, it is important to obtain a clear boundary in the topology optimization design result.

The method mainly used in the density approach of topology optimization is element density based topology optimization. Because the density is constant within the element, element density based method has a jagged boundary or smeared at the boundary. This jagged boundary also has difficulties in actual manufacturing. Also, it is not physically desirable. In the element-based density topology optimization, as the number of elements increases, the jagged boundary can be smoothed. As mesh becomes fine, the computational cost of optimization increases rapidly.

Various methods have been studied to solve such jagged boundaries problems. There are methods to reduce the number of elements used through an adaptive mesh refinement scheme [1]. Methodology of obtaining smooth boundaries using shape optimization after topology optimization ended [2]. In addition, a method of using a multiresolution scheme that distinguishes mesh discretization level was also studied [3]. In addition to these methodology, there is a level set method was proposed to get clear boundary [4]. The level set method expresses the geometry of the structure as an implicit function.

There is also methodology for represent the geometry of the structure by using iso-line. This methodology describes the boundary of the structure by using the iso-line of the physical quantity. Lee et al. proposed methodology which use nodal density variables and 0.5 threshold iso-line as post process

[5]. Victoria et al. proposed methodology using iso line with minimum criteria level [6]. This methodology changed the threshold value to satisfy the target volume. Abdi et al. proposed strain energy density iso-line for boundary representation with evolutionary topology optimization method [7].

In this study, iso-density line is used to represent the geometry of the structure. Design variables are directly updated with nodal density method. The author proposes modified stiffness matrix with penalty factor to prevent numerical instabilities. In addition, this proposed stiffness matrix is easy to implement. By using this modified stiffness matrix, strain energy term is considered when calculating sensitivity analysis. This term allows objective function to stably converge optimal design during the optimization procedure. Without mesh refinement scheme and post processing, this methodology represents continuous boundary which is optimum.

This paper is organized as follows. In chapter 2, this paper deals with research background such as structural optimization and density based topology optimization approach. In chapter 3, methodology is described to obtain a continuous boundary representation with iso-density line and modified stiffness matrix. In chapter 4, the proposed methodology was verified by solving numerical examples for the benchmark problem in topology optimization. In chapter 5, conclusion for this methodology is described and future works are also presented.



## **Chapter 2. Research background**

### **2.1. Structural optimization**

Prior to structural optimization, the design was mainly performed by the designer's intuition or experience. However, as the design of the structure became complicated, a systematic methodology for the optimal design of the structure was required. Structural Optimization began in 1904 when Michell published a paper about truss with minimum weight in the design domain [8]. During the past decades, many methods of structural optimization have been studied. Thus, as many studies have been conducted, structural optimization has played an important role in the design process.

There are three types of optimization methods for structural optimization. First, design variables in size optimization are the dimensions of the structure. Size optimization is an optimization method that determines dimensions without changing the shape and topology of structure. Shape optimization is a method to find optimum shape of member using the boundaries of the member as design variables. The size optimization and shape optimization in which the topology of the structure is determined in advance have limitations in the optimized results.

Topology optimization is an optimization technique that determines how materials are distributed [9]. This optimization method has no assumptions about the results of optimization, so it is possible to obtain an innovative design that was unexpected than other methods. Therefore topology optimization is mainly used in the conceptual design stage of structures.

## **2.2. Topology optimization method**

In the field of topology optimization, many studies have been conducted on the discrete structure and continuum structure. For studies on topology optimization of discrete structures, Rozbany and Prager have been extensively studied for decades [10].

### **2.2.1. Homogenization method**

The topology optimization methodology for the continuum structure was studied by Bendsoe and Kikuchi [11]. In this method, Bendsoe and Kikuchi introduced a microstructure with a rectangle structure. Then, the effective material properties were calculated through homogenization, which is a methodology to find relation between the modulus of elasticity and the density of a given material.

As the size and direction of the microstructure rectangle change, the microstructure distribution that minimize the objective function is optimized under a given boundary condition and load. In addition, Bendsoe introduced rank-2 material instead of microstructure with rectangle structure [12]. Bendsoe and Sigmund suggested the condition of power term that microstructure can make fictitious material of SIMP (Solid Isotropic Material with Penalization) [13].

### **2.2.2. ESO (Evolutionary Structural Optimization) method**

Xie and Steven proposed the ESO (Evolutionary Structural Optimization) method for topology optimization [14]. The presence of material is considered inefficient for elements subjected to low stress in the structure. By removing the materials of the inefficient elements, optimization is performed without additional sensitivity analysis. This ESO method has the advantage of simple concept and easy application. However, the disadvantage of this ESO method is that the removed elements are not regenerated.

Yang proposed the BESO (Bidirectional evolutionary method for stiffness optimization) algorithm for topology optimization [15]. BESO is an algorithm that is more advanced than the ESO algorithm. Inefficient elements are removed, efficient elements are added, and the optimal structure can be obtained gradually.

### 2.2.3. Level set method

Sethain and Wiegmann proposed a topology optimization method using the level set method [4]. Level set method topology optimization introduces a level set function. The presence or absence of a material is determined based on the zero contour of the level set function. Also, the zero contour of the level set function is determined as the boundary of the design. Because of these characteristics, the level set method can obtain clear boundary.

### 2.2.4. SIMP (Solid Isotropic Material with Penalization) method

Unlike the homogenization method, this method uses an explicit function for density and material properties without introducing microstructure [12]. If the density variable has an intermediate density other than 0 and 1, a penalty is applied to the material property.

Although it has the disadvantage of a little lack of mathematical rigor, this has the advantages of computational efficiency and easy implementation. This methodology is widely applied to various topology optimization problem. The formula of the classical SIMP method is as follows.

$$E_e(\rho_e) = (\rho_e)^p E_0, \quad \rho_e \in (0, 1] \quad (2.1)$$

$E_0$  is the stiffness of the material. Density value  $\rho_e$  has lower bound  $\rho_{\min}$ . This value allows small stiffness in the void region. Due to the stiffness in this void region, a singular problem does not occur during finite element analysis. Penalty factor  $p$  imposes a penalty so that an element with intermediate

density has less young's modulus. Modified SIMP approach is as follows.

$$E_e(\rho_e) = E_{\min} + \rho_e^p (E_0 - E_{\min}), \quad \rho_e \in [0, 1] \quad (2.2)$$

$E_{\min}$  means young's modulus of the element in void region. The modified SIMP method has the following advantages. In this modified SIMP approach, it is useful to implement in various filters and  $E_{\min}$  has a value regardless of the penalty factor.

## 2.3. Topology optimization formulation

### 2.3.1 Minimum compliance problem

Obtaining a structure with minimum compliance means obtaining a design that maximizes the stiffness of the structure. Obtaining the maximizing stiffness of structure while considering the limited amount of material used is one of the major issues in various engineering problems.

### 2.3.2 Mathematical formulation for the minimum compliance problem

The mathematical of topology optimization formulation for the minimum compliance problem is defined as follows.

$$\begin{aligned} \min_{\rho} : c(\rho) &= \mathbf{U}^T \mathbf{K} \mathbf{U} = \sum_{e=1}^N (\rho_e)^p \mathbf{u}_e^T \mathbf{k}_0 \mathbf{u}_e \\ s.t. : \sum_i \rho_i - V &\leq 0 \\ : \mathbf{K} \mathbf{U} &= \mathbf{f} \\ : 0 < \rho_{\min} &\leq \rho \leq 1 \end{aligned} \quad (2.3)$$

where  $c$  is compliance,  $\mathbf{K}$  is the global stiffness matrix,  $\mathbf{k}_0$  is the element stiffness matrix which has unit young's modulus material,  $\rho_e$  is element density,  $\mathbf{f}$  is load vector,  $\mathbf{U}$  is global

displacement vector,  $\mathbf{u}_e$  is element displacement vector,  $V$  is volume constraint.

The element stiffness matrix is defined as follows.

$$\mathbf{k}_e = \int \mathbf{B}^T \mathbf{C} \mathbf{B} d\Omega \quad (2.4)$$

$\mathbf{B}$  matrix means strain-displacement matrix and  $\mathbf{C}$  matrix is constitutive matrix. For a plane stress problem,  $\mathbf{C}$  matrix is defined as follows.

$$\mathbf{C} = \frac{E(\rho_e)}{1-\nu^2} \begin{pmatrix} 1 & \nu & 0 \\ \nu & 1 & 0 \\ 0 & 0 & \frac{1-\nu}{2} \end{pmatrix} \quad (2.5)$$

For gradient based optimization approach, sensitivity analysis is required. Objective function and constraint of sensitivities with respect to design variables can be calculated using the adjoint method. In general topology optimization problems, the number of design variables is much greater than the number of constraints. In such a case, the adjoint method is useful for sensitivity analysis.

$$\frac{\partial c}{\partial \rho_e} = -p(\rho_e)^{p-1} \mathbf{u}_e^T \mathbf{k}_0 \mathbf{u}_e \quad (2.6)$$

$$\frac{\partial V}{\partial \rho_e} = 1 \quad (2.7)$$

In Eq. (2.6), since the stiffness matrix is positive definite, it can be seen that the sensitivities of the objective function always has the same sign. This is one of the features of the minimum compliance problem. As the density of the material increases, the compliance decreases. This is also physically consistent. Eq. (2.7) is due to the assumption that the volume of all elements is one. Another feature is that the volume constraint is monotone and linear. Because of this characteristic, the minimum compliance problem can be solved relatively more easily than other topology optimization problems

such as compliant force inverter problem [16].

## 2.4. Optimizer for topology optimization

Topology optimization problem is one of the types of large-scale nonlinear problems. Various optimizers have been studied to solve the topology optimization problem. A comparison of the wide range of optimizers is well researched in the following paper [17].

### 2.4.1. Optimality criteria method

The Optimality Criteria (OC) method is one of the widely used method of solving structural optimization problems. Bendsøe proposed a heuristic method to update design variables as follows [18].

$$\rho_e^{\text{new}} = \begin{cases} \max(0, \rho_e - m) & \text{if } \rho_e B_e^\eta \leq \max(0, \rho_e - m) \\ \min(1, \rho_e + m) & \text{if } \rho_e B_e^\eta \geq \min(1, \rho_e + m) \\ \rho_e B_e^\eta & \text{otherwise} \end{cases} \quad (2.8)$$

where  $m$  is move limit and  $\eta$  is damping coefficient. The roles of move limit and damping coefficient prevent rapid design variable update.  $B_e$  can be calculated from the Eq. (2.9).

$$B_e = -\frac{\partial c}{\partial \rho_e} \left( \lambda \frac{\partial V}{\partial \rho_e} \right)^{-1} \quad (2.9)$$

$\lambda$  is Lagrange multiplier value which is satisfied volume constraint. This value of  $\lambda$  can be obtained with bi-section method or other numerical algorithms.

### 2.4.2. The method of moving asymptotes

Since Svanverg proposed the method of moving asymptotes (MMA) algorithm in 1987, this algorithm

has become a widely used algorithm for structural optimization [19]. The MMA algorithm is particularly effective when there are many design variables compared to constraints. In the MMA algorithm, the objective function of the given nonlinear optimization and the constraint are approximated by a convex function. The convex function is approximated using the gradient value of the current iteration and moving asymptotes parameter information.

The approximated function is defined as Eq. (2.10).

$$f_i^{(k)}(\mathbf{x}) = r_i^{(k)} + \sum_{j=1}^n \left( \frac{p_{ij}^{(k)}}{U_j^{(k)} - x_j} + \frac{q_{ij}^{(k)}}{x_j - L_j^{(k)}} \right) \quad \text{for each } i = 0, 1, \dots, m \quad (2.10)$$

where  $p_{ij}^{(k)}$  and  $q_{ij}^{(k)}$  are defined as Eqs. (2.11) - (2.13),  $k$  is the iteration number of optimization,  $j$  means the number of design variables.

$$\text{if } \partial f_i / \partial x_j > 0 \text{ then } p_{ij}^{(k)} = (U_j^{(k)} - x_j^{(k)})^2 \partial f_i / \partial x_j \text{ and } q_{ij}^{(k)} = 0. \quad (2.11)$$

$$\text{if } \partial f_i / \partial x_j < 0 \text{ then } q_{ij}^{(k)} = -(x_j^{(k)} - L_j^{(k)})^2 \partial f_i / \partial x_j \text{ and } p_{ij}^{(k)} = 0. \quad (2.12)$$

$$\text{if } \partial f_i / \partial x_j = 0 \text{ then } q_{ij}^{(k)} = p_{ij}^{(k)} = 0. \quad (2.13)$$

$$r_i^{(k)} = f_i^{(k)}(\mathbf{x}) - \sum_{j=1}^n \left( \frac{p_{ij}^{(k)}}{U_j^{(k)} - x_j} + \frac{q_{ij}^{(k)}}{x_j - L_j^{(k)}} \right) \quad (2.14)$$

A new iteration point can be obtained by solving the sub problem using approximated objective functions and constraints. Then this new iteration point can be used to create a sub problem.

The process of solving these sub problems and generating them is repeated until the stopping criteria are satisfied.

## 2.5. Filtering scheme

In density based topology optimization, various filtering schemes have been studied to avoid the numerical instabilities such as checkerboard pattern and mesh dependency. A checker board pattern means that the black and white elements are repeated so that it looks like a checker board pattern. The mesh dependency problem means that the result of topology optimization obtained depends on the degree of discretization of the mesh. To solve these numerical instabilities problem, a higher order element or restriction method must be used. Among the restriction methods, filtering scheme is widely used because it is easy to implement and simple.

### 2.5.1 Sensitivity filter

Sigmund proposed the sensitivity filtering scheme to avoid numerical instabilities [20]. This sensitivity filter is defined as follows.

$$\frac{\widehat{\partial c}}{\partial \rho_e} = \frac{\sum_{i \in N_e} w(\mathbf{x}_i) \rho_i \frac{\partial c}{\partial \rho_i}}{\rho_e \sum_{i \in N_e} w(\mathbf{x}_i)} \quad (2.15)$$

where  $\frac{\partial c}{\partial \rho_i}$  is the original sensitivities,  $\frac{\widehat{\partial c}}{\partial \rho_e}$  is modified sensitivities,  $N_e$  is the set of elements within the filter radius from the center of element e.  $w(\mathbf{x}_i)$  is a weight function and is defined as follows.

$$w(\mathbf{x}_i) = r_{\min} - \|\mathbf{x}_i - \mathbf{x}_e\| \quad (2.16)$$

where  $r_{\min}$  is filter radius,  $\mathbf{x}_i$  and  $\mathbf{x}_e$  are the position of the centers of each element e and i.



In the modified SIMP formulation, unlike the classic SIMP method, the value of the design variable can be 0. If the density value of design variable is less than  $\gamma$ ,  $\gamma$  is used instead of the density value to avoid singularity. Usually, the value of  $\gamma$  is 0.001. So the Eq. (2.17) is used for modified SIMP method.

$$\frac{\widehat{\partial c}}{\partial \rho_e} = \frac{\sum_{i \in N_e} w(\mathbf{x}_i) \rho_i \frac{\partial c}{\partial \rho_i}}{\max(\rho_e, \gamma) \sum_{i \in N_e} w(\mathbf{x}_i)} \quad (2.17)$$

### 2.5.2 Density filter

Density filter was proposed by Bruns, Tortorelli and Borudín[21-22]. The density filter modifies the original density using the following equation.

$$\widetilde{\rho}_e = \frac{\sum_{i \in N_e} w(\mathbf{x}_i) \rho_i}{\sum_{i \in N_e} w(\mathbf{x}_i)} \quad (2.18)$$


The important thing in this equation is that  $\widetilde{\rho}_e$  is the physical density variables.  $\rho_e$  has no longer a physical meaning, it only functions as an intermediate density. Therefore, volume constraints must be calculated as variables that have physical meaning. Sensitivities can be obtained with Eq (2.19) by using chain rule.

$$\frac{\partial \psi}{\partial \rho_j} = \sum_{i \in N_e} \frac{\partial \psi}{\partial \widetilde{\rho}_e} \frac{\partial \widetilde{\rho}_e}{\partial \rho_j} \quad (2.19)$$

where  $\psi$  is compliance or volume constraint.

### 2.5.3. Heaviside projection filter

The above-described sensitivity filter and density filter have the advantage of being easy to implement, but when these filters are used, the density variable has an intermediate value. In particular, the intermediate density at the boundary has no physical meaning and it is difficult to recognize the boundary. Guest proposed the following filter with Heaviside step function to obtain the 0-1 solution [23]. The Heaviside step function is replaced with the following function along with the continuation scheme and parameter  $\beta$ .

$$\bar{\rho}_e = 1 - e^{-\beta \tilde{\rho}_e} + \tilde{\rho}_e e^{-\beta} \quad (2.20)$$

where  $\tilde{\rho}_e$  is filtered density with density filter and  $\bar{\rho}_e$  is physical density with projection filter. Eq. (2.20) approximates the Heaviside projection function as  $\beta$  increases. Since nonlinearity increases as the approximation to the Heaviside projection filter increases, a continuation scheme that gradually increases value of  $\beta$  should be used. The sensitivities value with respect to the intermediate density variable can be obtained using the chain rule.

$$\frac{\partial c}{\partial \tilde{\rho}_j} = \sum_{i \in N_e} \frac{\partial c}{\partial \bar{\rho}_e} \frac{\partial \bar{\rho}_e}{\partial \tilde{\rho}_j} \quad (2.21)$$

## 2.5.4. Alternative sensitivity filter

Alternative sensitivity filter is proposed by Borrvall [24]. The purpose of this filter is to get 0-1 solutions by modifying the original sensitivity filter. Original sensitivity filter is modified as follows Eq. (2.22). This filter is not a mesh independent filter. However, by using this alternative sensitivity filter, a discrete solution can be obtained.

$$\frac{\tilde{\partial c}}{\partial \rho_e} = \frac{\sum_{i \in N_e} w(\mathbf{x}_i) \rho_i \frac{\partial c}{\partial \rho_i}}{\sum_{i \in N_e} \rho_i w(\mathbf{x}_i)} \quad (2.22)$$

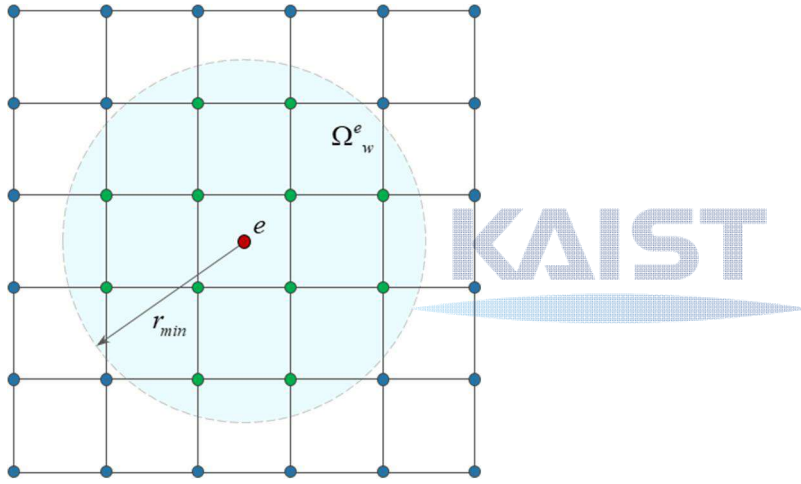


Fig. 2.1 Projection scheme within filter radius from element e

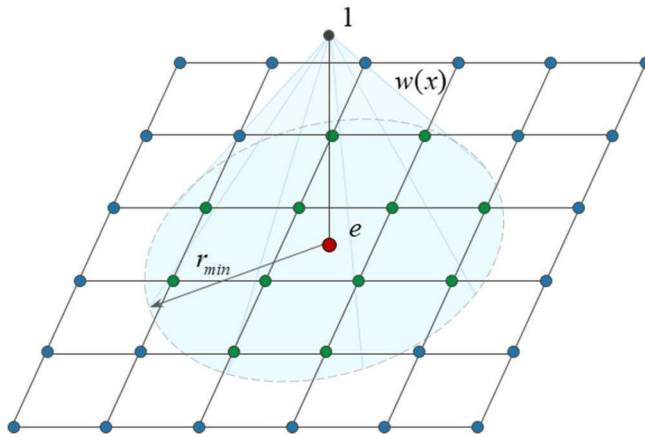


Fig. 2.2 Linear projection scheme weight function

## 2.6. Introduction of iso-density line

Nodal density is design variables in the element and have values from  $\rho_{\min}$  to 1. To avoid singularity,  $\rho_{\min}$  was implemented. Using a linear interpolation method, an element is divided based on the point at which the density equals the threshold value. **Fig 2.3** shows how to divide elements into solid and void domain using interpolation of nodal density. A black node has a density value greater than the threshold value. A gray node has a density value less than the threshold value. The dark area means the solid domain and light gray area means the void domain. The shape that can be expressed differs depending on the location of the node that exceeds the threshold value.

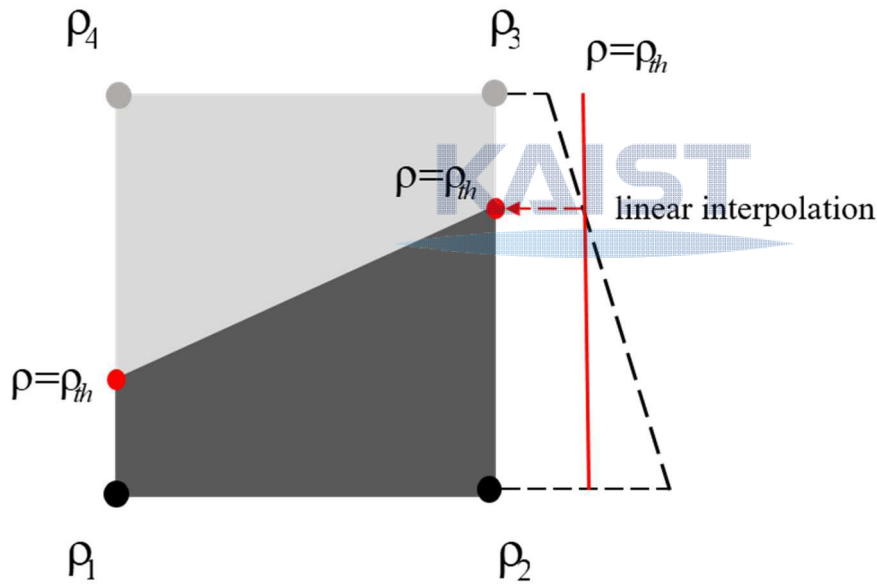


Fig. 2.3 Implementation of iso-density line

Lorensen proposed marching cube algorithm [25]. Marching square algorithm is an algorithm that considers the marching cube algorithm in two dimensions. The marching squares algorithm gives case of contour line. **Fig 2.4** shows 16 cases using the Marching square algorithm. Cases 5 and 10 have ambiguous cases because of their symmetry. As can be seen in **Fig 2.5**, This was classified using the average of the nodal density.

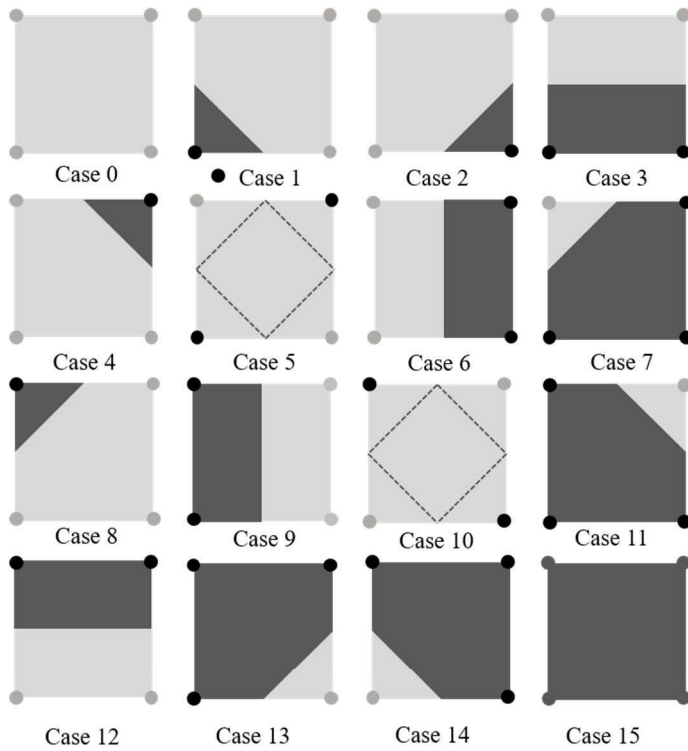


Fig. 2.4 Iso-density line case in marching square algorithm

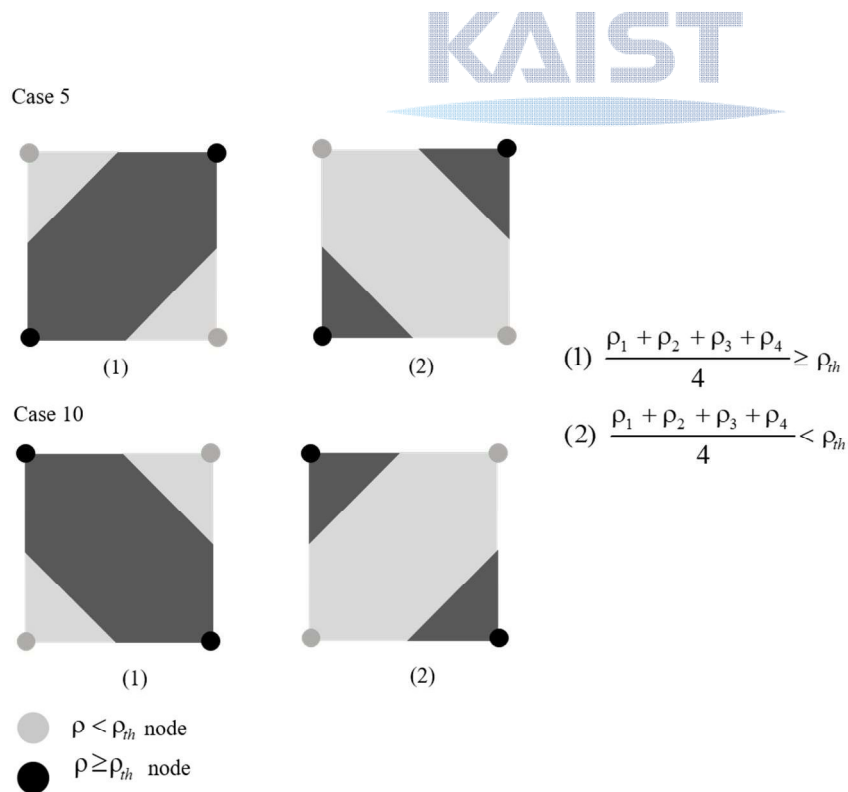


Fig. 2.5 Ambiguous case in marching square algorithm

**Fig 2.6** shows a typical case of how the domain of an element can be divided. There is triangle, quadrilateral, pentagon, two triangles, and hexagon domains. For other cases, it can be obtained by rotating cases in **Fig 2.6**. Therefore, Numerical integration for stiffness matrix and sensitivity analysis were calculated only in the case of **Fig 2.6** in this thesis.

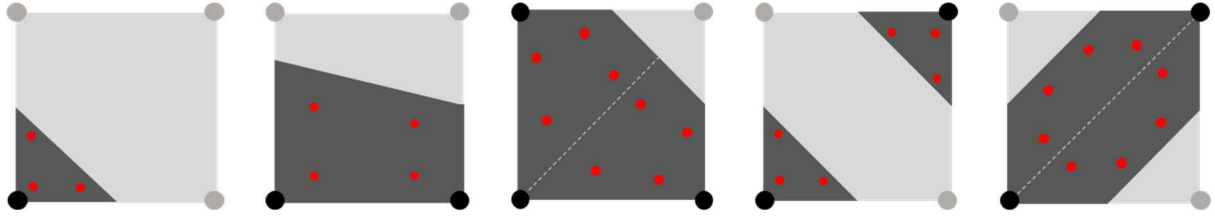


Fig. 2.6 Typical case of divided domain

## 2.7. Numerical integration scheme

Stiffness matrix can be calculated using Eqs. (2.23-2.24). The subscript s means solid and v means void domain. Because  $C_v$  is related to young's modulus and it has negligible value, the integral function is calculated only in the solid domain. The advantage of this strategy is that there is no need for a re-meshing technique. This method of calculating the stiffness of the sub domain has been applied in extended finite element method or fluid structure interaction problems. [26-27]. The red point means gauss point in solid domain.

$$\mathbf{k}_e = \int \mathbf{B}^T \mathbf{C} \mathbf{B} d\Omega \quad (2.23)$$

$$\mathbf{k}_e = \int \mathbf{B}^T \mathbf{C}_s \mathbf{B} d\Omega_s + \int \mathbf{B}^T \mathbf{C}_v \mathbf{B} d\Omega_v \quad (2.24)$$

### 2.7.1. Triangle domain

This method integrates the integrand in a given domain by performing mapping twice with two natural coordinates. In physical coordinates, the mesh of an element is a square with length 1. In natural coordinate  $\xi - \eta$ , the mesh size is a square of size 2. The stiffness matrix calculation for triangle

domain is defined as follows Eq. (2.25)

$$\mathbf{k}_e = \frac{1}{2} \sum_{i=1}^3 \mathbf{B}(\xi_i^g, \eta_i^g)^T \mathbf{C} \mathbf{B}(\xi_i^g, \eta_i^g) w_i \det(\mathbf{J}_p) \det(\mathbf{J}_q) \quad (2.25)$$

$$\mathbf{J}_p = \begin{pmatrix} \frac{\partial x}{\partial \xi} & \frac{\partial y}{\partial \xi} \\ \frac{\partial x}{\partial \eta} & \frac{\partial y}{\partial \eta} \end{pmatrix} = \begin{pmatrix} \frac{1}{2} & 0 \\ 0 & \frac{1}{2} \end{pmatrix} \quad (2.26)$$

$$\begin{aligned} \xi &= r\xi_1 + s\xi_2 + (1-r-s)\xi_3 \\ \eta &= r\eta_1 + s\eta_2 + (1-r-s)\eta_3 \end{aligned} \quad (2.27)$$

$$\mathbf{J}_q = \begin{pmatrix} \frac{\partial \xi}{\partial r} & \frac{\partial \eta}{\partial r} \\ \frac{\partial \xi}{\partial s} & \frac{\partial \eta}{\partial s} \end{pmatrix} = \begin{pmatrix} \xi_1 - \xi_3 & \eta_1 - \eta_3 \\ \xi_2 - \xi_3 & \eta_2 - \eta_3 \end{pmatrix} \quad (2.28)$$

$$\xi_i^g = \xi(r_i^g, s_i^g), \eta_i^g = \eta(r_i^g, s_i^g) \quad (2.29)$$

where  $r_i^g, s_i^g$  are gauss points of the triangular domain in r-s natural coordinates.  $w_i$  is weight factors of triangle element.  $\xi_i^g, \eta_i^g$  are points that are mapped to gauss points in r-s natural coordinates and these values can be obtained using Eq. (2.27). Jacobian matrices  $\mathbf{J}_p$  and  $\mathbf{J}_q$  can be obtained by using the Eq. (2.26) and Eq. (2.28)

### 2.7.2. Quadrilateral domain

Like the triangle domain, it can be obtained using mapping. This method integrates the integrand in a given domain by performing mapping twice with two natural coordinates. The stiffness matrix calculation for triangle domain is defined as follows Eq. (2.30)

$$\mathbf{k}_e = \sum_{i=1}^4 \mathbf{B}(\xi_i^g, \eta_i^g)^T \mathbf{C} \mathbf{B}(\xi_i^g, \eta_i^g) \det(\mathbf{J}_p) \det(\mathbf{J}_q) \quad (2.30)$$

Jacobian matrix  $\mathbf{J}_p$  is the same as previously defined as Eq. (2.26). Jacobian matrix  $\mathbf{J}_q$  is a function of  $r$  and  $s$ .

$$\mathbf{J}_q = \begin{pmatrix} \frac{\partial \xi}{\partial r} & \frac{\partial \eta}{\partial r} \\ \frac{\partial \xi}{\partial s} & \frac{\partial \eta}{\partial s} \end{pmatrix} \quad (2.31)$$

$$\begin{aligned} \xi &= \sum_{i=1}^4 h_i(r, s) \xi_i \\ \eta &= \sum_{i=1}^4 h_i(r, s) \eta_i \end{aligned} \quad (2.32)$$

where  $h_i(r, s)$  is shape function of bi-linear four node element in  $r$ - $s$  coordinate. The stiffness matrix of the quadrilateral domain can also be obtained similarly to the method described above.

### 2.7.3. Other domains

For pentagon, two triangles and hexagon domain, the stiffness matrix can be calculated by dividing the triangle and quadrilateral sub-domains.  $\mathbf{k}_{quad}$  means element stiffness matrix for quadrilateral domain.

$\mathbf{k}_{tri}$  means element stiffness matrix for triangle domain.

#### 2.7.3.1 Pentagon domain

$$\mathbf{k}_e = \mathbf{k}_{quad1} + \mathbf{k}_{quad2} \quad (2.33)$$

#### 2.7.3.2 Two triangles domain

$$\mathbf{k}_e = \mathbf{k}_{tri1} + \mathbf{k}_{tri2} \quad (2.34)$$



### 2.7.3.3 Hexagon domain

$$\mathbf{k}_e = \mathbf{k}_{quad1} + \mathbf{k}_{quad2} \quad (2.35)$$

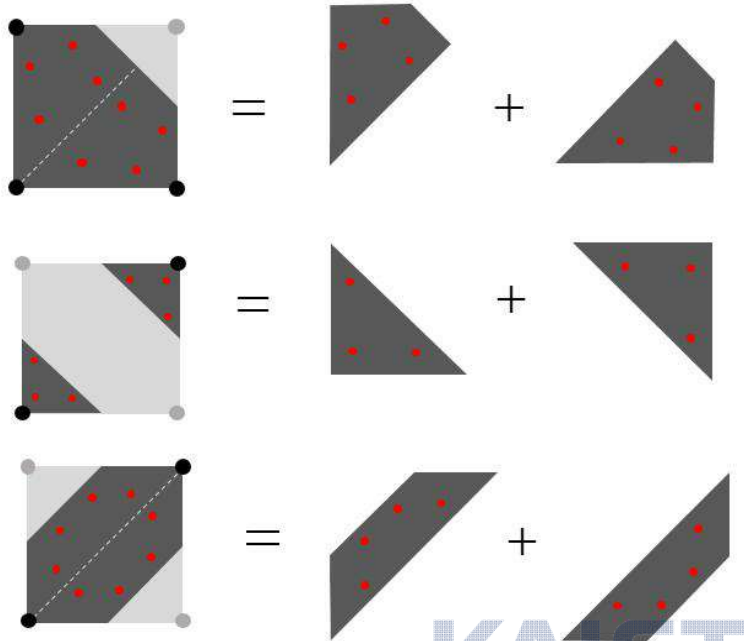


Fig. 2.7 Summation of domain for stiffness calculation

## Chapter 3. Nodal density based topology optimization

To have a continuous boundary representation, nodal density based approach was implemented. The iso-density line was used to represent boundary. Each node was used as a design variable and optimization performed. Based on an arbitrary threshold value, the element by linear interpolation along the edges was divided into solid and void regions by linear interpolation scheme. The stiffness of only the part where the material exists was calculated and implemented into the optimization procedure. To enable objective function more stable convergence, the proposed stiffness matrix was modified with penalty factor.

### 3.1. Formulation of proposed method for minimum compliance

In this research, modified stiffness matrix is proposed in the equation (3.1).  $\bar{\rho}_e$  is the average of the node density in an element. Using this modified stiffness matrix, this formulation has the advantage of being able to stably converge during the optimization process.

$$\mathbf{k}_m = (\bar{\rho}_e)^p \mathbf{k}_e \quad (3.1)$$

where  $\mathbf{k}_e$  is the stiffness matrix of element considering only the solid region.  $\mathbf{k}_m$  means modified stiffness matrix with penalty factor.  $p$  means penalty factor.

In the case of minimum compliance problem, the problem is defined as follows Eq. (3.2)

$$\begin{aligned} \min_{\rho} : C(\rho) &= \mathbf{U}^T \mathbf{K} \mathbf{U} = \sum_{e=1}^N (\bar{\rho}_e)^p \mathbf{u}_e^T \mathbf{k}_e \mathbf{u}_e \\ \text{s.t.} : \sum_i \rho_i - V &\leq 0 \\ : \mathbf{K} \mathbf{U} &= \mathbf{f} \\ : 0 < \rho_{\min} &\leq \rho \leq 1 \end{aligned} \quad (3.2)$$

Sensitivity formulation can be obtained using adjoint method.

$$\frac{\partial c}{\partial \rho_i} = \sum_{e \in \Omega_i} -\frac{p}{4} (\bar{\rho}_e)^{p-1} \mathbf{u}_e^T \mathbf{k}_e \mathbf{u}_e - \mathbf{u}_e^T (\bar{\rho}_e)^p \frac{\partial \mathbf{k}_e}{\partial \rho_i} \mathbf{u}_e \quad (3.3)$$

Domain  $\Omega_i$  is a set of elements with the i-th design variable as a node. As can be seen in **Fig 3.1**, The number of elements in the domain set is three cases.

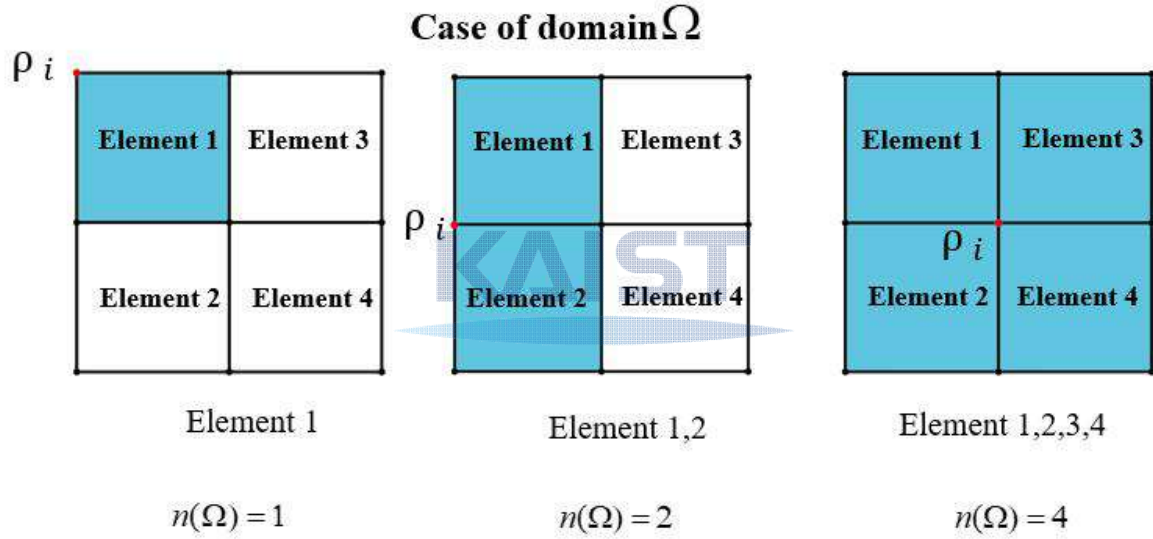


Fig. 3.1 Case of domain set

### 3.2. Sensitivity Analysis

The sensitivity can be calculated by a semi-analytic method. When performing sensitivity analysis, it is assumed that the domain case does not change even if the design variable changes. Because sensitivities implies a change in the objective function with respect to infinitesimal change of design variables, this assumption is reasonable. This assumption makes the sensitivity analysis easier.

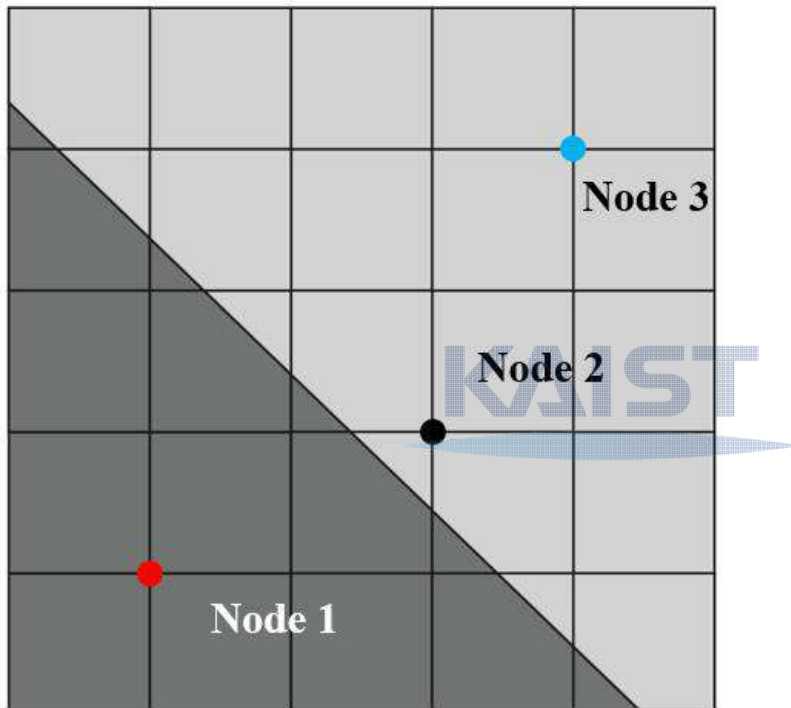


Fig. 3.2 Case for location of node

Node 1 means that all elements of the domain sets  $\Omega$  are solid region. Node 3 means that all elements of the domain sets  $\Omega$  are void region. The element of the domain set of Node2 has solid and void regions. Without modified stiffness matrix, sensitivity analysis formulation is as follows.

$$\frac{\partial c}{\partial \rho_i} = \sum_{e \in \Omega_i} -\mathbf{u}_e^T \frac{\partial \mathbf{k}_e}{\partial \rho_i} \mathbf{u}_e \quad (3.4)$$

This term is the derivative of the stiffness matrix of the design variable. This term is zero where e-th element is solid element or void element. When the case for location of node is 1 or 3, this term is zero due to the aforementioned assumption. During optimization, convergence may be difficult because there is no difference in the sensitivity of the node in solid and void elements. When the case for location of node is only 2, sensitivity has not zero values. This leads to numerical instabilities.

With the proposed modified stiffness, sensitivity formulation is Eq. (3.3). The first term in the modified sensitivity formulation is related to strain energy term. The second term is the derivative of the stiffness matrix of the design variables. With the strain energy term, the sensitivity of the solid region can be obtained higher than that of the void region. It is physically more meaningful that the sensitivity in the solid region is greater than that in the void region. Nodal design variables converge to 0-1 easily due to the penalty factor. Because design variables converge to 0-1, the aforementioned assumptions make it more reasonable.

KAIST

Derivatives of stiffness matrix with respect to design variables can be obtained by using chain rule as follows Eq. (3.5)

$$\frac{\partial \mathbf{k}_e}{\partial \rho_i} = \sum_j \frac{\partial \mathbf{k}_e}{\partial x_j^*} \frac{\partial x_j^*}{\partial \rho_i} + \frac{\partial \mathbf{k}_e}{\partial y_j^*} \frac{\partial y_j^*}{\partial \rho_i} \quad (3.5)$$

The physical volume can be obtained by calculating the area of the solid domain within an element.

$$V_e = V_e(\rho_1, \rho_2, \rho_3, \rho_4) \quad (3.6)$$

The derivative of volume constraint can be calculated using chain rule as follows Eq. (3.7)

$$\begin{aligned} \frac{\partial V}{\partial \rho_i} &= \sum_{e \in \Omega_i} \frac{\partial V_e}{\partial \rho_i} \\ \frac{\partial V_e}{\partial \rho_i} &= \sum_j \frac{\partial V_e}{\partial x_j^*} \frac{\partial x_j^*}{\partial \rho_i} + \frac{\partial V_e}{\partial y_j^*} \frac{\partial y_j^*}{\partial \rho_i} \end{aligned} \quad (3.7)$$

### 3.2.1. Derivatives of stiffness matrix for triangle domain

Derivatives of stiffness matrix for triangle domain can be obtained by using Eq. (3.5). As can be seen in the **Fig 3.3** and Eq. (3.8), the stiffness matrix is a function of the point determined by iso-density line. Superscript \* means that the point can be moved by the density values of the node.

$$\mathbf{k}_e = \mathbf{k}_e(x_2^*, y_3^*) \quad (3.8)$$

$$\begin{aligned} \frac{\partial \mathbf{k}_e}{\partial \rho_1} &= \frac{\partial \mathbf{k}_e}{\partial x_2^*} \frac{\partial x_2^*}{\partial \rho_1} + \frac{\partial \mathbf{k}_e}{\partial y_3^*} \frac{\partial y_3^*}{\partial \rho_1} \\ \frac{\partial \mathbf{k}_e}{\partial \rho_2} &= \frac{\partial \mathbf{k}_e}{\partial x_2^*} \frac{\partial x_2^*}{\partial \rho_2} + \frac{\partial \mathbf{k}_e}{\partial y_3^*} \frac{\partial y_3^*}{\partial \rho_2} \\ \frac{\partial \mathbf{k}_e}{\partial \rho_3} &= \frac{\partial \mathbf{k}_e}{\partial x_2^*} \frac{\partial x_2^*}{\partial \rho_3} + \frac{\partial \mathbf{k}_e}{\partial y_3^*} \frac{\partial y_3^*}{\partial \rho_3} \\ \frac{\partial \mathbf{k}_e}{\partial \rho_4} &= \frac{\partial \mathbf{k}_e}{\partial x_2^*} \frac{\partial x_2^*}{\partial \rho_4} + \frac{\partial \mathbf{k}_e}{\partial y_3^*} \frac{\partial y_3^*}{\partial \rho_4} \end{aligned} \quad (3.9)$$


In the case of local node 3, it can be seen that even if the density value of node 3 changes, there is no change in the value of the stiffness matrix. It means that sensitivity with respect to node 3 is zero.

### 3.2.2. Derivatives of stiffness matrix for quadrilateral domain

As can be seen in the **Fig 3.4** and Eq. (3.10), the stiffness matrix is a function of the following variables.

$$\mathbf{k}_e = \mathbf{k}_e(y_3^*, y_4^*) \quad (3.10)$$

$$\begin{aligned}
\frac{\partial \mathbf{k}_e}{\partial \rho_1} &= \frac{\partial \mathbf{k}_e}{\partial y_3^*} \frac{\partial y_3^*}{\partial \rho_1} + \frac{\partial \mathbf{k}_e}{\partial y_4^*} \frac{\partial y_4^*}{\partial \rho_1} \\
\frac{\partial \mathbf{k}_e}{\partial \rho_2} &= \frac{\partial \mathbf{k}_e}{\partial y_3^*} \frac{\partial y_3^*}{\partial \rho_2} + \frac{\partial \mathbf{k}_e}{\partial y_4^*} \frac{\partial y_4^*}{\partial \rho_2} \\
\frac{\partial \mathbf{k}_e}{\partial \rho_3} &= \frac{\partial \mathbf{k}_e}{\partial y_3^*} \frac{\partial y_3^*}{\partial \rho_3} + \frac{\partial \mathbf{k}_e}{\partial y_4^*} \frac{\partial y_4^*}{\partial \rho_3} \\
\frac{\partial \mathbf{k}_e}{\partial \rho_4} &= \frac{\partial \mathbf{k}_e}{\partial y_3^*} \frac{\partial y_3^*}{\partial \rho_4} + \frac{\partial \mathbf{k}_e}{\partial y_4^*} \frac{\partial y_4^*}{\partial \rho_4}
\end{aligned} \tag{3.11}$$

### 3.2.3. Derivatives of stiffness matrix for pentagon domain

As can be seen in the **Fig 3.5** and Eq. (3.12), the stiffness matrix is a function of the following variables.

$$\mathbf{k}_e = \mathbf{k}_e(x_{3\_d1}^*, y_{3\_d2}^*) \tag{3.12}$$

$$\begin{aligned}
\frac{\partial \mathbf{k}_e}{\partial \rho_1} &= \frac{\partial \mathbf{k}_e}{\partial x_{3\_d1}^*} \frac{\partial x_{3\_d1}^*}{\partial \rho_1} + \frac{\partial \mathbf{k}_e}{\partial y_{3\_d2}^*} \frac{\partial y_{3\_d2}^*}{\partial \rho_1} \\
\frac{\partial \mathbf{k}_e}{\partial \rho_2} &= \frac{\partial \mathbf{k}_e}{\partial x_{3\_d1}^*} \frac{\partial x_{3\_d1}^*}{\partial \rho_2} + \frac{\partial \mathbf{k}_e}{\partial y_{3\_d2}^*} \frac{\partial y_{3\_d2}^*}{\partial \rho_2} \\
\frac{\partial \mathbf{k}_e}{\partial \rho_3} &= \frac{\partial \mathbf{k}_e}{\partial x_{3\_d1}^*} \frac{\partial x_{3\_d1}^*}{\partial \rho_3} + \frac{\partial \mathbf{k}_e}{\partial y_{3\_d2}^*} \frac{\partial y_{3\_d2}^*}{\partial \rho_3} \\
\frac{\partial \mathbf{k}_e}{\partial \rho_4} &= \frac{\partial \mathbf{k}_e}{\partial x_{3\_d1}^*} \frac{\partial x_{3\_d1}^*}{\partial \rho_4} + \frac{\partial \mathbf{k}_e}{\partial y_{3\_d2}^*} \frac{\partial y_{3\_d2}^*}{\partial \rho_4}
\end{aligned} \tag{3.13}$$

In the case of local node 1, it can be seen that even if the density value of node 1 changes, there is no change in the value of the stiffness matrix. It means that sensitivity with respect to node 1 is zero.

### 3.2.4. Derivatives of stiffness matrix for two triangles domain

As can be seen in the **Fig 3.5** and Eq. (3.14), the stiffness matrix is a function of the following variables.

$$\mathbf{k}_e = \mathbf{k}_e(x_{2\_d1}^*, y_{3\_d1}^*, x_{3\_d2}^*, y_{1\_d2}^*) \quad (3.14)$$

$$\begin{aligned} \frac{\partial \mathbf{k}_e}{\partial \rho_1} &= \frac{\partial \mathbf{k}_e}{\partial x_{2\_d1}^*} \frac{\partial x_{2\_d1}^*}{\partial \rho_1} + \frac{\partial \mathbf{k}_e}{\partial x_{3\_d2}^*} \frac{\partial x_{3\_d2}^*}{\partial \rho_1} + \frac{\partial \mathbf{k}_e}{\partial y_{3\_d1}^*} \frac{\partial y_{3\_d1}^*}{\partial \rho_1} + \frac{\partial \mathbf{k}_e}{\partial y_{1\_d2}^*} \frac{\partial y_{1\_d2}^*}{\partial \rho_1} \\ \frac{\partial \mathbf{k}_e}{\partial \rho_2} &= \frac{\partial \mathbf{k}_e}{\partial x_{2\_d1}^*} \frac{\partial x_{2\_d1}^*}{\partial \rho_2} + \frac{\partial \mathbf{k}_e}{\partial x_{3\_d2}^*} \frac{\partial x_{3\_d2}^*}{\partial \rho_2} + \frac{\partial \mathbf{k}_e}{\partial y_{3\_d1}^*} \frac{\partial y_{3\_d1}^*}{\partial \rho_2} + \frac{\partial \mathbf{k}_e}{\partial y_{1\_d2}^*} \frac{\partial y_{1\_d2}^*}{\partial \rho_2} \\ \frac{\partial \mathbf{k}_e}{\partial \rho_3} &= \frac{\partial \mathbf{k}_e}{\partial x_{2\_d1}^*} \frac{\partial x_{2\_d1}^*}{\partial \rho_3} + \frac{\partial \mathbf{k}_e}{\partial x_{3\_d2}^*} \frac{\partial x_{3\_d2}^*}{\partial \rho_3} + \frac{\partial \mathbf{k}_e}{\partial y_{3\_d1}^*} \frac{\partial y_{3\_d1}^*}{\partial \rho_3} + \frac{\partial \mathbf{k}_e}{\partial y_{1\_d2}^*} \frac{\partial y_{1\_d2}^*}{\partial \rho_3} \\ \frac{\partial \mathbf{k}_e}{\partial \rho_4} &= \frac{\partial \mathbf{k}_e}{\partial x_{2\_d1}^*} \frac{\partial x_{2\_d1}^*}{\partial \rho_4} + \frac{\partial \mathbf{k}_e}{\partial x_{3\_d2}^*} \frac{\partial x_{3\_d2}^*}{\partial \rho_4} + \frac{\partial \mathbf{k}_e}{\partial y_{3\_d1}^*} \frac{\partial y_{3\_d1}^*}{\partial \rho_4} + \frac{\partial \mathbf{k}_e}{\partial y_{1\_d2}^*} \frac{\partial y_{1\_d2}^*}{\partial \rho_4} \end{aligned} \quad (3.15)$$

### 3.2.5. Derivatives of stiffness matrix for hexagon domain

As can be seen in the **Fig 3.6** and Eq. (3.16), the stiffness matrix is a function of the following variables.

$$\mathbf{k}_e = \mathbf{k}_e(x_{3\_d1}^*, y_{4\_d1}^*, x_{2\_d2}^*, y_{3\_d2}^*) \quad (3.16)$$

$$\begin{aligned} \frac{\partial \mathbf{k}_e}{\partial \rho_1} &= \frac{\partial \mathbf{k}_e}{\partial x_{3\_d1}^*} \frac{\partial x_{3\_d1}^*}{\partial \rho_1} + \frac{\partial \mathbf{k}_e}{\partial x_{2\_d2}^*} \frac{\partial x_{2\_d2}^*}{\partial \rho_1} + \frac{\partial \mathbf{k}_e}{\partial y_{4\_d1}^*} \frac{\partial y_{4\_d1}^*}{\partial \rho_1} + \frac{\partial \mathbf{k}_e}{\partial y_{3\_d2}^*} \frac{\partial y_{3\_d2}^*}{\partial \rho_1} \\ \frac{\partial \mathbf{k}_e}{\partial \rho_2} &= \frac{\partial \mathbf{k}_e}{\partial x_{3\_d1}^*} \frac{\partial x_{3\_d1}^*}{\partial \rho_2} + \frac{\partial \mathbf{k}_e}{\partial x_{2\_d2}^*} \frac{\partial x_{2\_d2}^*}{\partial \rho_2} + \frac{\partial \mathbf{k}_e}{\partial y_{4\_d1}^*} \frac{\partial y_{4\_d1}^*}{\partial \rho_2} + \frac{\partial \mathbf{k}_e}{\partial y_{3\_d2}^*} \frac{\partial y_{3\_d2}^*}{\partial \rho_2} \\ \frac{\partial \mathbf{k}_e}{\partial \rho_3} &= \frac{\partial \mathbf{k}_e}{\partial x_{3\_d1}^*} \frac{\partial x_{3\_d1}^*}{\partial \rho_3} + \frac{\partial \mathbf{k}_e}{\partial x_{2\_d2}^*} \frac{\partial x_{2\_d2}^*}{\partial \rho_3} + \frac{\partial \mathbf{k}_e}{\partial y_{4\_d1}^*} \frac{\partial y_{4\_d1}^*}{\partial \rho_3} + \frac{\partial \mathbf{k}_e}{\partial y_{3\_d2}^*} \frac{\partial y_{3\_d2}^*}{\partial \rho_3} \\ \frac{\partial \mathbf{k}_e}{\partial \rho_4} &= \frac{\partial \mathbf{k}_e}{\partial x_{3\_d1}^*} \frac{\partial x_{3\_d1}^*}{\partial \rho_4} + \frac{\partial \mathbf{k}_e}{\partial x_{2\_d2}^*} \frac{\partial x_{2\_d2}^*}{\partial \rho_4} + \frac{\partial \mathbf{k}_e}{\partial y_{4\_d1}^*} \frac{\partial y_{4\_d1}^*}{\partial \rho_4} + \frac{\partial \mathbf{k}_e}{\partial y_{3\_d2}^*} \frac{\partial y_{3\_d2}^*}{\partial \rho_4} \end{aligned} \quad (3.17)$$



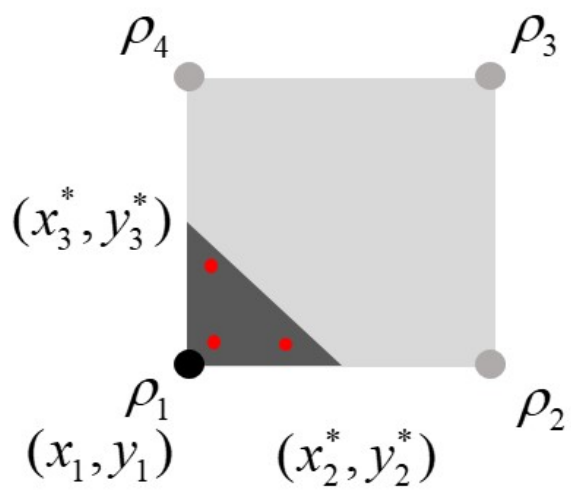


Fig. 3.3 Triangle domain

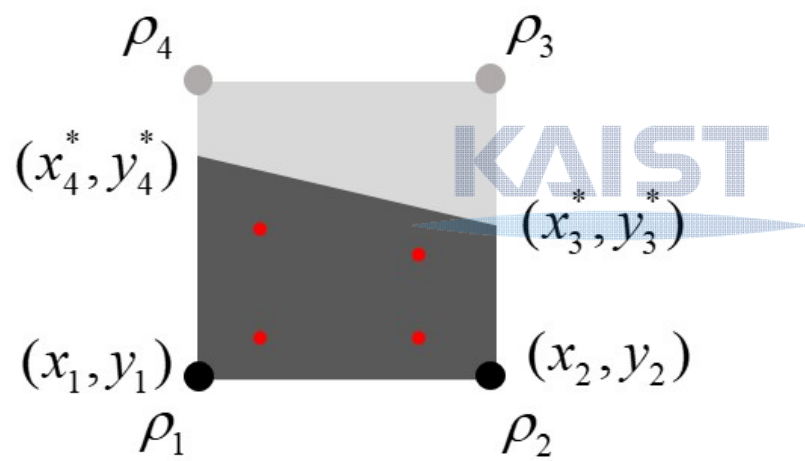


Fig. 3.4 Quadrilateral domain

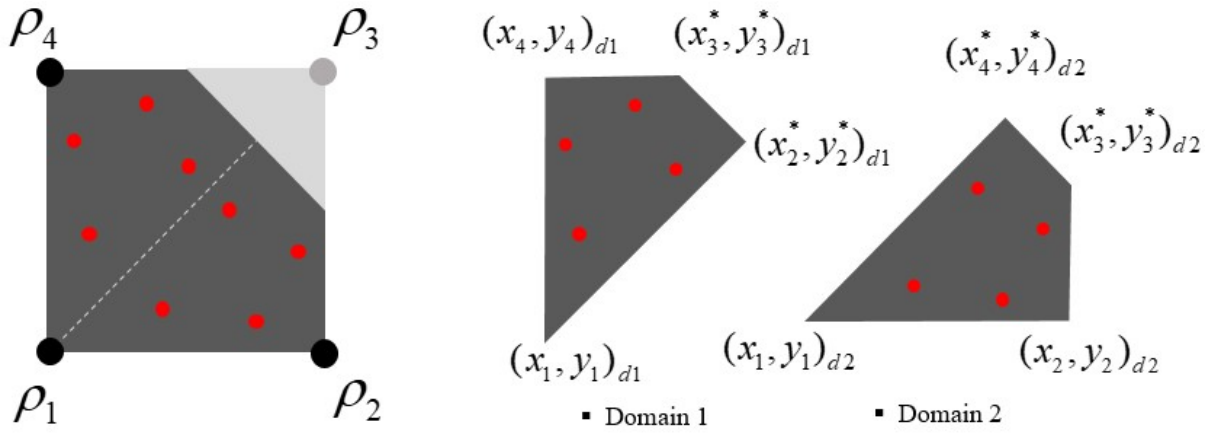


Fig. 3.5 Pentagon domain

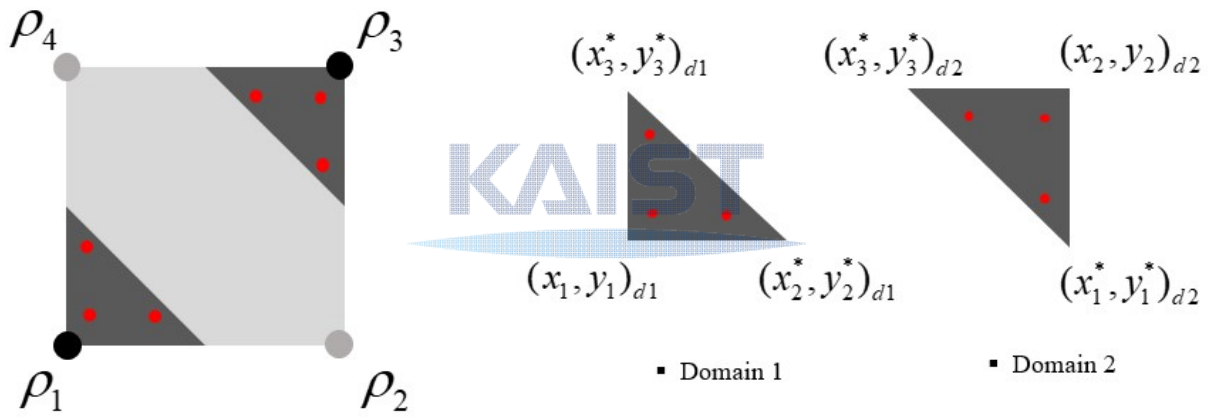


Fig. 3.6 Two triangles domain

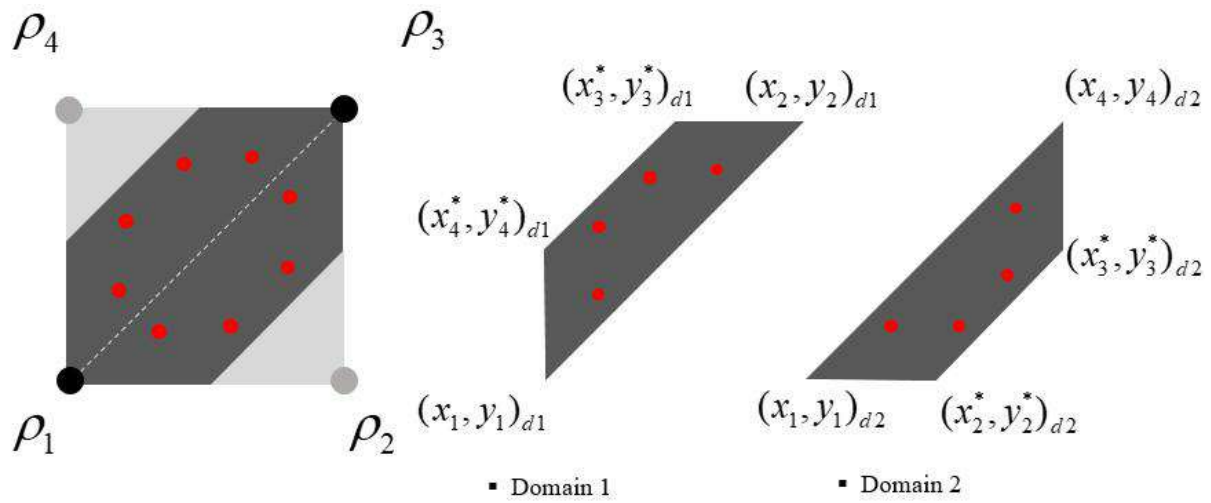


Fig. 3.7 Hexagon domain

### 3.3. Optimization Procedure

Proposed methodology is as shown in **Fig 3.8**. This proposed methodology used a penalty factor with stiffness matrix to avoid numerical instabilities. However, This methodology leads to an underestimation of the stiffness of the structure. This stiffness underestimation is because the stiffness matrix of the element in the boundary is penalized. After optimization is completed, compliance is obtained through finite element analysis using the original stiffness matrix without penalization. This compliance does not underestimate the effect of the stiffness of elements in the boundary. In order to distinguish between the compliance  $c(\rho)$  obtained during the optimization process and the compliance  $\tilde{c}(\rho_{opt})$  after optimization, the former was named as nominal compliance and the latter as physical compliance. Obviously physical compliance  $\tilde{c}$  is not an optimal value because it is not the objective function of the original problem. Nevertheless, it provides physical meaning about optimized result  $\rho_{opt}$ .

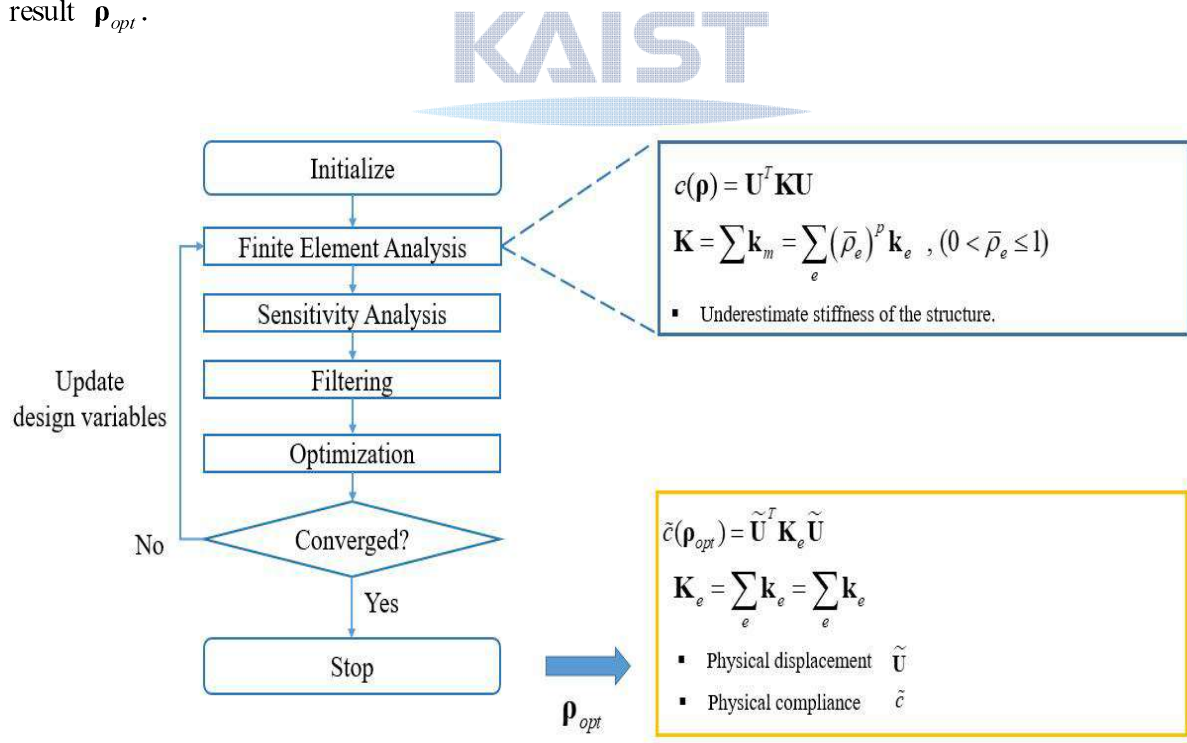


Fig. 3.8 Procedure of topology optimization

## Chapter 4. Numerical example

In chapter 4, verification of the proposed methodology is dealt with through numerical examples widely used in topology optimization. The young's modulus of the material  $E_0$  is one. Poisson ratio is 0.3. Magnitude of load is one. The initial input for every problem in this study has the density uniformly arranged in the domain as shown in **Fig 4.2**. It gives 50% volume in domain at initial design. Penalty factor  $p$  is 4. MMA optimizer is used in this study.

### 4.1. MBB beam problem

The boundary condition and loading given in MBB Beam are as follows.



Fig. 4.1. MBB beam problem

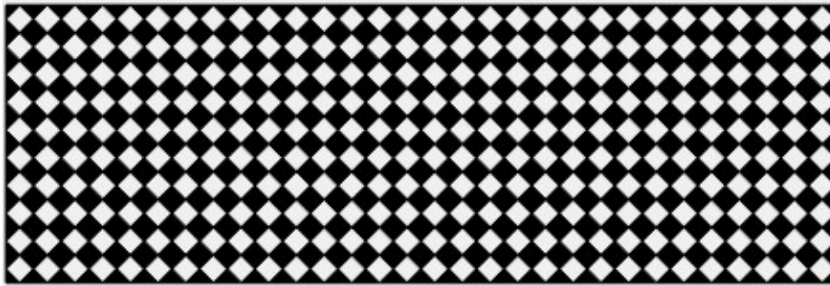


Fig. 4.2. Initial design for optimization

Sigmund introduced measure of discreteness to evaluate the degree of discreteness of an optimized design [29].

$$M_{nd} = \frac{\sum_{e=1}^n 4\rho_e(1-\rho_e)}{n} \times 100 (\%) \quad (4.1)$$

If the element density is 0 or 1, the measure of discreteness is 0. It can be seen that well discretized design has small  $M_{nd}$  value. In the proposed method, there is no intermediate density within an element, so the Eq. (4.1) cannot be used exactly. Instead, this measure of discreteness equation is slightly modified to evaluate the degree of penalized stiffness of an optimized design in Eq. (4.2). As shown in **Fig 3.9** elements with intermediate volumes are penalized for stiffness like intermediate density.

$$M_{nd} = \frac{\sum_{e=1}^n 4V_e(1-V_e)}{n} \times 100 (\%) \quad (4.2)$$


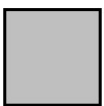
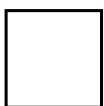



SIMP method		
$\rho_e = 1$	$\rho_e = 0.5$	$\rho_e = 0$
		
Proposed method		
$V_e = 1$	$V_e = 0.5$	$V_e = 0$
		
$M_{nd} = 0$	$M_{nd} = 1$	$M_{nd} = 0$

Fig. 4.3 Measure of discreteness of both method

In these examples with proposed method, alternative sensitivity filter was used. It was shown that the alternative sensitivity filter can be more stable than the commonly used sensitivity filter and density filter during the optimization procedure. This is because a more 0-1 solution can be obtained by using an alternative sensitivity filter. This clear 0-1 solution is far from the threshold density value of 0.5. So the optimization process using alternative sensitivity filtering is more stable. In particular, density filter is more unstable than alternative sensitivity filtering because it has the effect of directly smoothing the density variables.

Table 4.1. MBB problem comparison for 60×20 elements

		<b>Proposed method</b>	<b>Reference (SIMP)</b>
Number of finite elements		1,200 (60×20)	1,200 (60×20)
Number of design variables		1,281	1,200
Filter radius		1.5	1.5
Compliance	Nominal	221.1699	190.4210
	Physical	(170.8496)	-
Volume fraction		0.5	0.5
Measure of discreteness (%)		11.08	0.003
Computational cost	Iteration	135	374
	CPU time	48.5 s	17.12 s

Table 4.2. MBB problem comparison for 90×30 elements

		<b>Proposed method</b>	<b>Reference (SIMP)</b>
Number of finite elements		2,700 (90×30)	2,700 (90×30)
Number of design variables		2,821	2,700
Filter radius		2.25	2.25
Compliance	Nominal	209.2133	191.8124
	Physical	(172.1187)	-
Volume fraction		0.5	0.5
Measure of discreteness (%)		7.61	1.68
Computational cost	Iteration	142	455
	CPU time	137.40 s	31.65 s

Table 4.3. MBB problem comparison for 120×40 elements

		Proposed method	Reference (SIMP)
Number of finite elements		4,800 (120×40)	4,800 (120×40)
Number of design variables		4,961	4,800
Filter radius		3	3
Compliance	Nominal	207.3335	191.0176
	Physical	(172.8602)	-
Volume fraction		0.5	0.5
Measure of discreteness (%)		5.96	0.93
Computational cost	Iteration	42	405
	CPU time	74.88 s	55.38 s

Table 4.4. MBB problem comparison for 180×60 elements

		Proposed method	Reference (SIMP)
Number of finite elements		10,800 (180×60)	10,800 (180×60)
Number of design variables		11,041	10,800
Filter radius		4.5	4.5
Compliance	Nominal	204.2535	191.8497
	Physical	(173.9615)	-
Volume fraction		0.5	0.5
Measure of discreteness (%)		3.83	1.288
Computational cost	Iteration	315	491
	CPU time	1324.11 s	120.41 s

Reference (SIMP) method used heaviside projection filter to compare with the proposed method with binary density in elements. As can be seen from the **Table 4.1** to **Table 4.4**, proposed method has higher compliance than SIMP method. However, this is due to the underestimation of the stiffness of the element in the boundary. As the mesh becomes finer, it can be seen that measure of discreteness decreases. Therefore, the nominal compliance also decrease. Without underestimation of stiffness of structure, it can be seen that physical compliance has a lower value than the objective function of the reference.

## 4.2. Cantilever beam problem

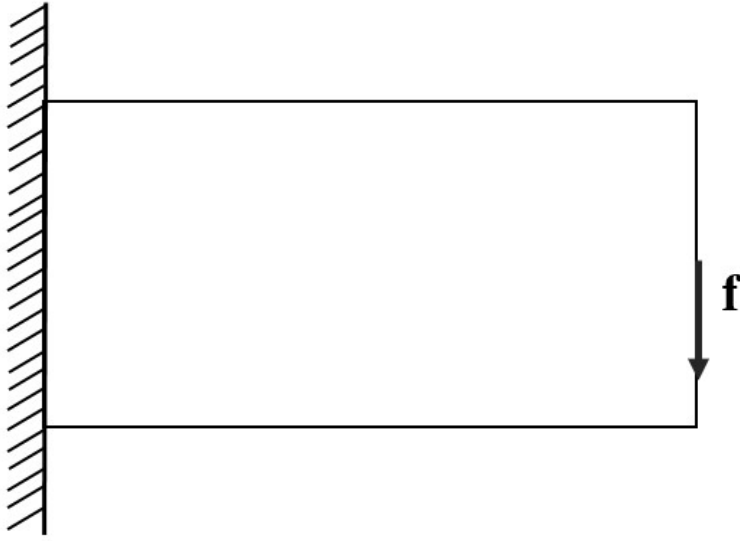


Fig. 4.4. Cantilever beam problem

Table 4.5. Cantilever problem comparison for  $60 \times 30$  elements

		Proposed method	Reference (SIMP)
Number of finite elements		1,800 ( $60 \times 30$ )	1,800 ( $60 \times 30$ )
Number of design variables		1,891	1,800
Filter radius		1.5	1.5
Compliance	Nominal	70.6597	62.6725
	Physical	(56.4067)	-
Volume fraction		0.5	0.5
Measure of discreteness (%)		9.95	0.006
Computational cost	Iteration	58	324
	CPU time	33.10 s	20.97 s

The boundary condition and loading for cantilever beam problem is given in **Fig 4.4**. As shown **Table 4.5**, **Table 4.6**, **Table 4.7**, and **Table 4.8**, it can be seen that the objective function is minimized and the given volume constraint (50%) is satisfied. In addition, it can be seen that the nominal compliance decreases with the measure discreteness value. Physical compliance has a lower value than reference method.



Table 4.6. Cantilever problem comparison for 80×40 elements

		<b>Proposed method</b>	<b>Reference (SIMP)</b>
Number of finite elements		3,200 (80×40)	3,200 (80×40)
Number of design variables		3,321	3,200
Filter radius		2	2
Compliance	Nominal	68.2973	62.0119
	Physical	(56.5161)	-
Volume fraction		0.5	0.5
Measure of discreteness (%)		7.68	0.032
Computational cost	Iteration	82	324
	CPU time	89.89 s	30.80 s

Table 4.7. Cantilever problem comparison for 100×50 elements

		<b>Proposed method</b>	<b>Reference (SIMP)</b>
Number of finite elements		5,000 (100×50)	5,000 (100×50)
Number of design variables		5,151	5,000
Filter radius		2.5	2.5
Compliance	Nominal	68.2439	61.8712
	Physical	(57.0602)	-
Volume fraction		0.5	0.5
Measure of discreteness (%)		5.71	0.143
Computational cost	Iteration	47	393
	CPU time	94.86 s	44.58 s

Table 4.8. Cantilever problem comparison for 120× 60 elements

		<b>Proposed method</b>	<b>Reference (SIMP)</b>
Number of finite elements		7,200 (120×60)	7,200 (120×60)
Number of design variables		7,381	7,200
Filter radius		3	3
Compliance	Nominal	67.6001	62.0856
	Physical	(57.1781)	-
Volume fraction		0.5	0.5
Measure of discreteness (%)		5.04	0.629
Computational cost	Iteration	80	374
	CPU time	227.13 s	59.09 s

### 4.3. Michell type structure problem

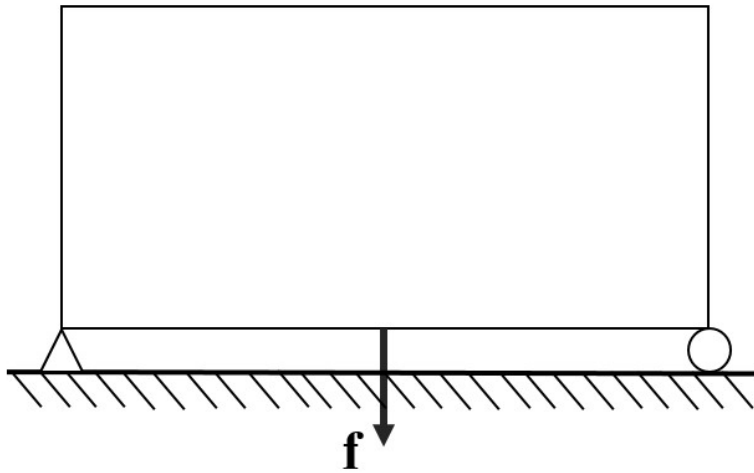


Fig. 4.5. Michell type structure problem

Table 4.9. Michell type structure problem comparison for  $60 \times 30$  elements

		Proposed method	Reference (SIMP)
Number of finite elements		1,800 ( $60 \times 30$ )	1,800 ( $60 \times 30$ )
Number of design variables		1,891	1,800
Filter radius		1.5	1.5
Compliance	Nominal	19.6787	15.9945
	Physical	(12.8967)	-
Volume fraction		0.25	0.25
Measure of discreteness (%)		7.92	0.050
Computational cost	Iteration	60	307
	CPU time	34.22 s	21.21 s

The boundary condition and loading for Michell type problem is given in **Fig 4.5**. As shown **Table 4.9**, **Table 4.10**, **Table 4.11**, and **Table 4.12**, it can be seen that the objective function is minimized. Initial design for optimization is uniformly distributed with 50% volume fraction as shown in **Fig 4.2** within a given domain. As optimization proceeds, the given volume constraint 25% is satisfied. In addition, it can be seen that the nominal compliance decreases with the measure discreteness value. Physical compliance has a lower value than reference method.

Table 4.10. Michell type structure problem comparison for 80× 40 elements

		Proposed method	Reference (SIMP)
Number of finite elements		3,200 (80×40)	3,200 (80×40)
Number of design variables		3,321	3,200
Filter radius		2	2
Compliance	Nominal	18.9196	16.2285
	Physical	(13.2522)	-
Volume fraction		0.25	0.25
Measure of discreteness (%)		5.94	0.036
Computational cost	Iteration	83	261
	CPU time	90.98 s	20.17 s

Table 4.11. Michell type structure problem comparison for 100× 50 elements

		Proposed method	Reference (SIMP)
Number of finite elements		5,000 (100×50)	5,000 (100×50)
Number of design variables		5,151	5,000
Filter radius		2.5	2.5
Compliance	Nominal	18.8622	16.3738
	Physical	(13.5942)	-
Volume fraction		0.25	0.25
Measure of discreteness (%)		4.82	0.076
Computational cost	Iteration	51	427
	CPU time	92.69 s	63.43 s

Table 4.12. Michell type structure problem comparison for 120× 60 elements

		Proposed method	Reference (SIMP)
Number of finite elements		7,200 (120×60)	7,200 (120×60)
Number of design variables		7,381	7,200
Filter radius		3	3
Compliance	Nominal	18.7169	16.7660
	Physical	(13.8478)	-
Volume fraction		0.25	0.25
Measure of discreteness (%)		3.99	0.948
Computational cost	Iteration	60	402
	CPU time	174.61 s	76.16 s

As the mesh became finer, the objective function decreased. If the domain is discretized with coarse mesh, the ratio of the stiffness subjected to penalized element at the boundary is larger, so the compliance is higher in the coarse mesh. If domain is discretized with fine mesh, the ratio can be reduced. Therefore, compliance is lower in fine mesh than in coarse mesh. Optimization results and iterative process can be seen from **Fig.4.6** to **Fig.4.41**. It can be seen that the proposed method satisfies the volume constraint and makes objective function converges stably.

Computational cost is heavier than SIMP method. This is because the two methods differ in calculating stiffness. However, even after the optimization of the SIMP method is finished, the jagged boundary still remains due to the characteristics of the element density method. This proposed method is meaningful because the boundary expression is continuous and there is no intermediate density. In addition, when comparing the physical compliance and the compliance of the SIMP method, it can be seen that the physical compliance has a smaller value. This means that the optimized design with proposed method puts the material more optimally within the domain than the SIMP method.

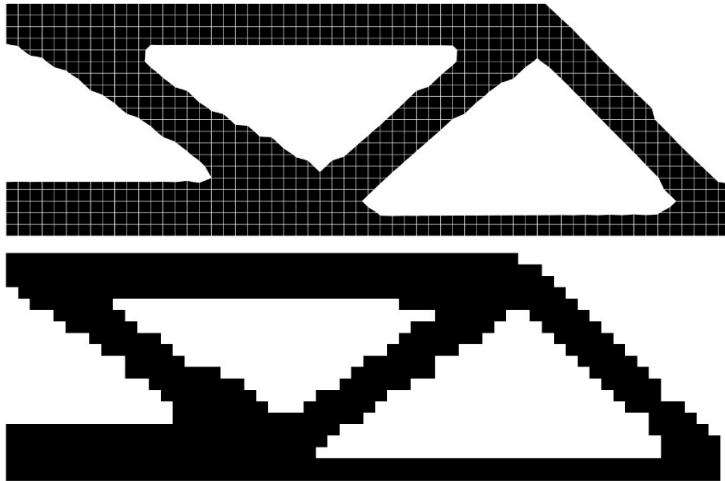


Fig. 4.6. 60×20 MBB beam problem Proposed method (top) and SIMP method (bottom)

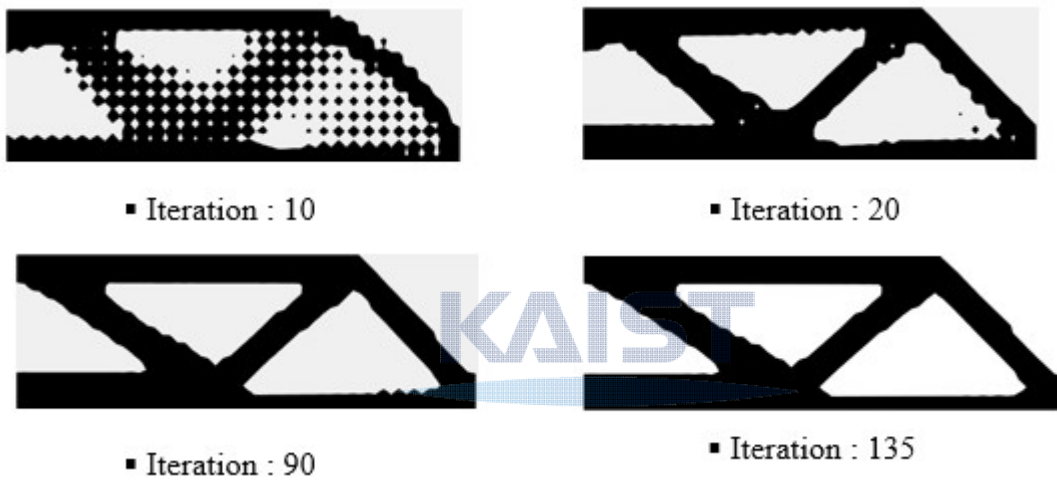


Fig. 4.7. Iterative process of 60×20 elements

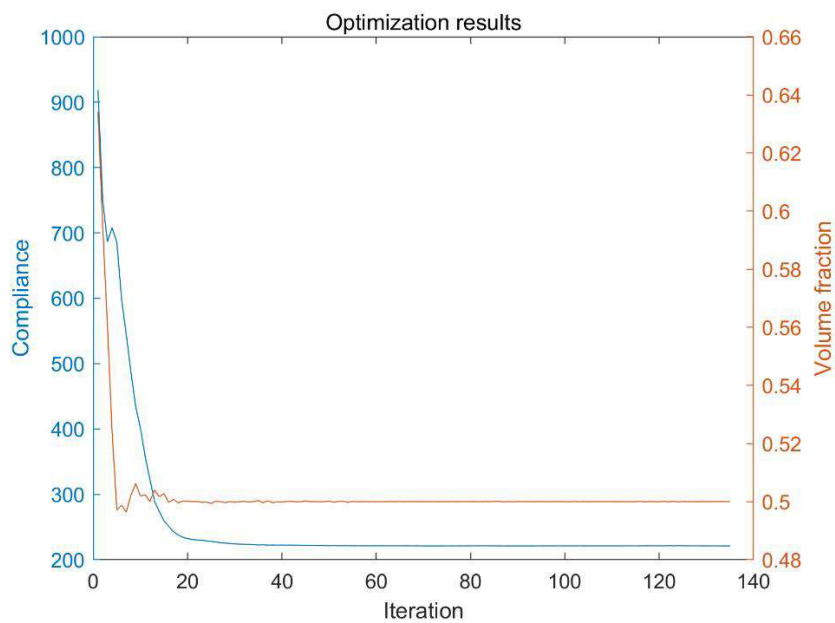


Fig. 4.8. Optimization results for 60×20 elements

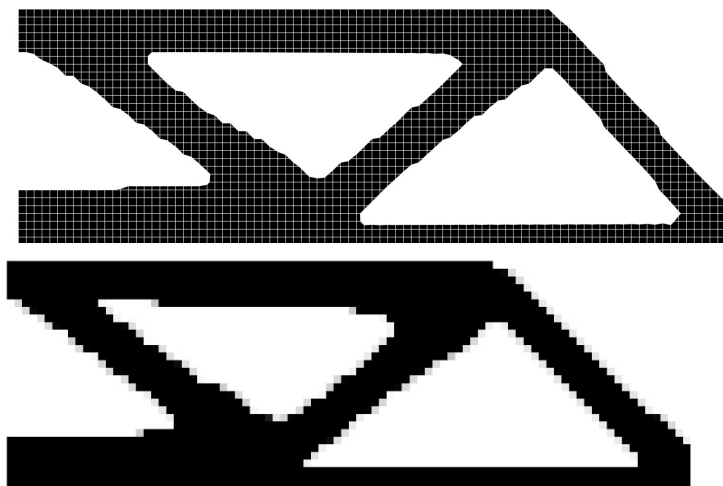


Fig. 4.9. 90×30 MBB beam problem Proposed method (top) and SIMP method (bottom)

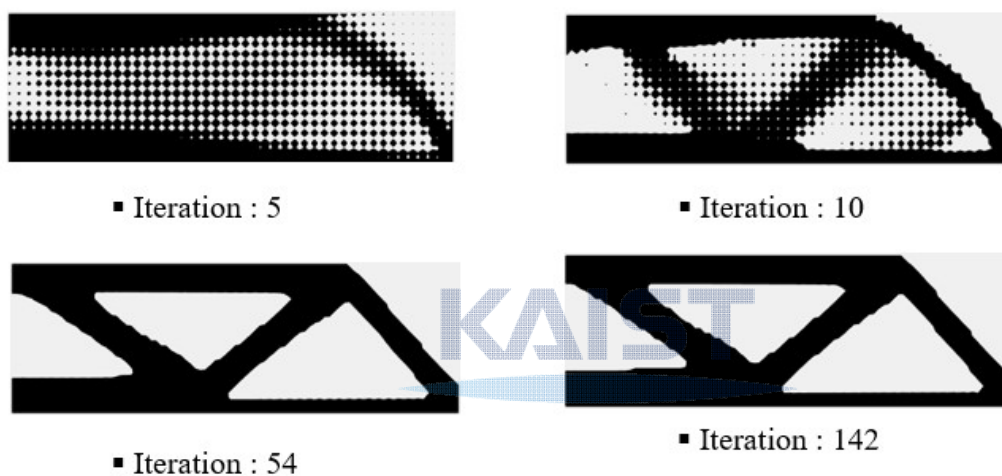


Fig. 4.10. Iterative process of 90×30 elements

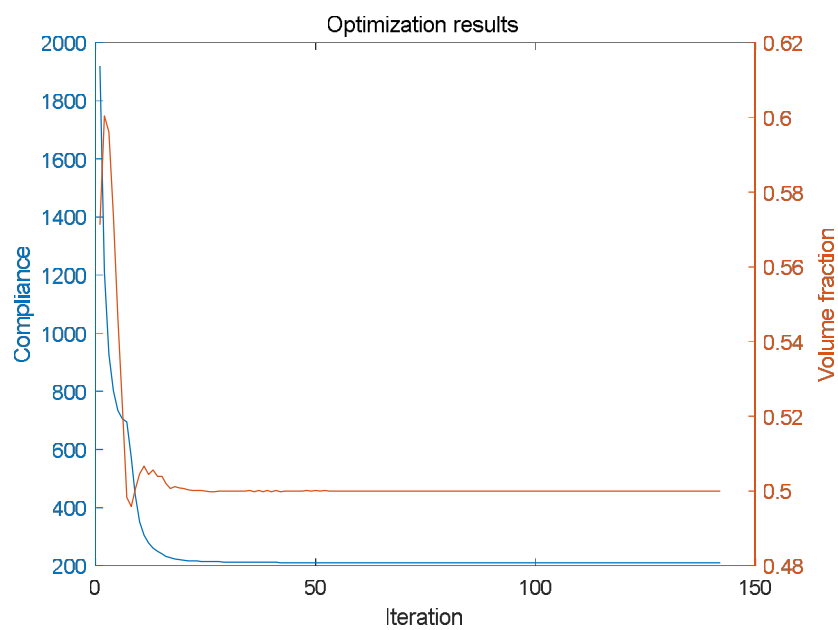


Fig. 4.11. Optimization results for 90×30 elements

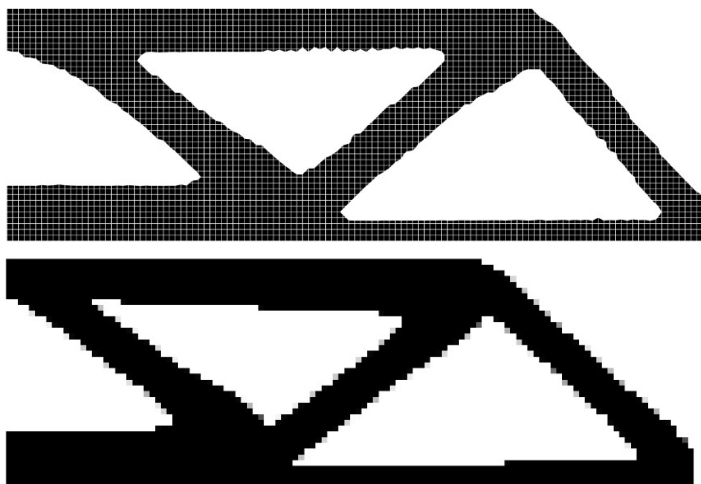


Fig. 4.12. 120×40 MBB beam problem proposed method (top) and SIMP method (bottom)

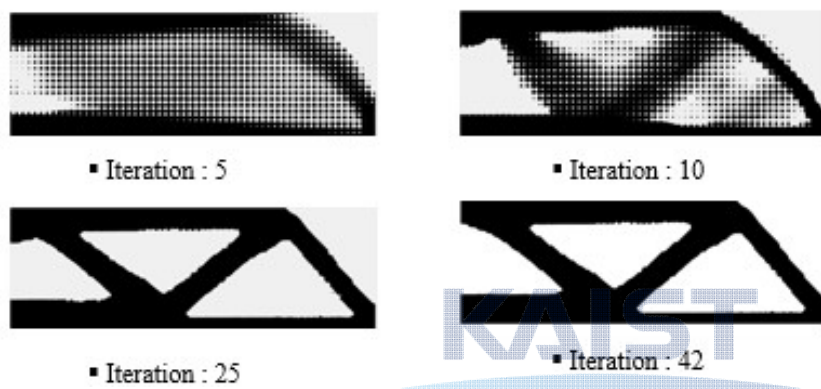


Fig. 4.13. Iterative process of 120×40 elements

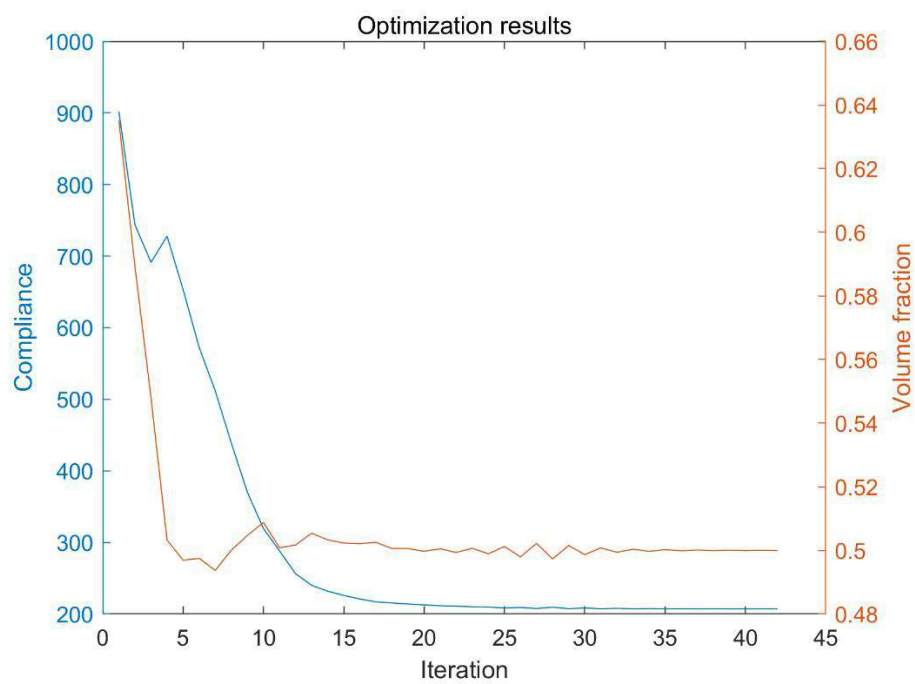


Fig. 4.14. Optimization results for 120×40 elements



Fig. 4.15. 180×60 MBB beam problem proposed method (top) and SIMP method (bottom)

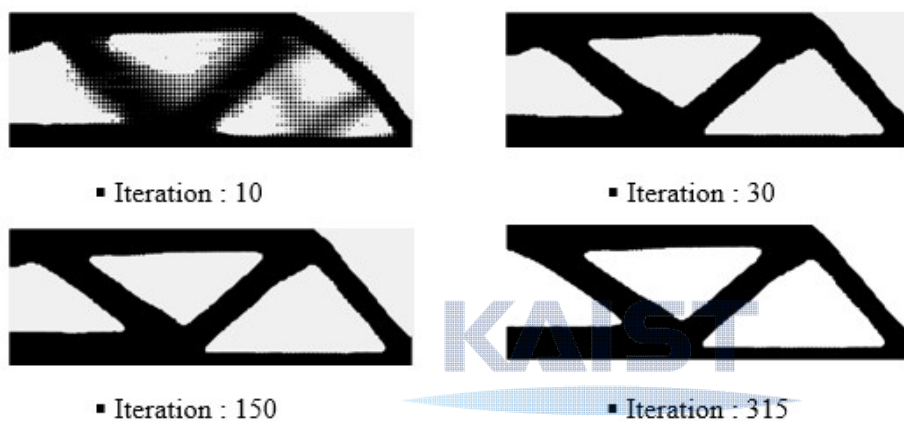


Fig. 4.16. Iterative process of 180×60 elements

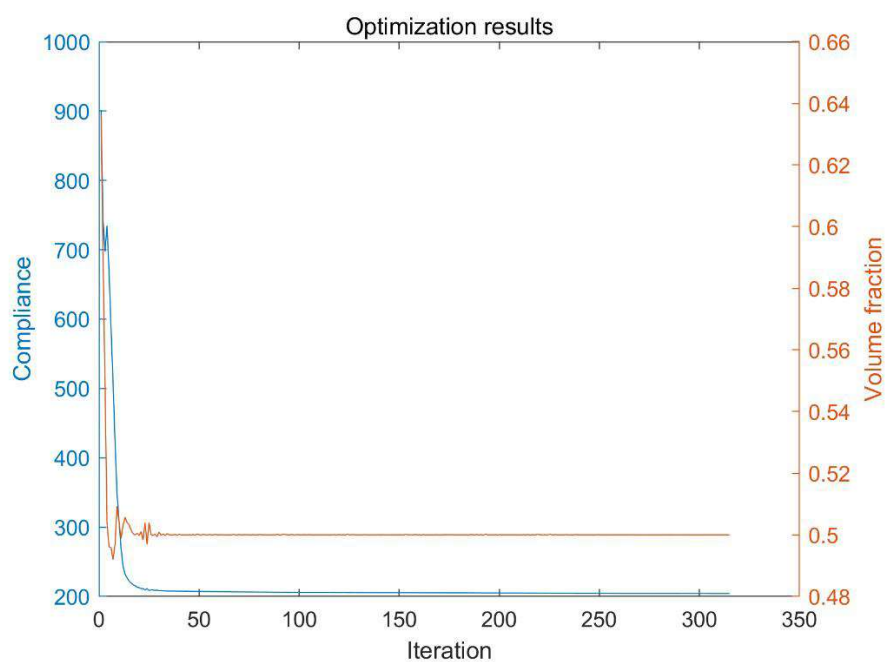


Fig. 4.17. Optimization results for 180×60 elements



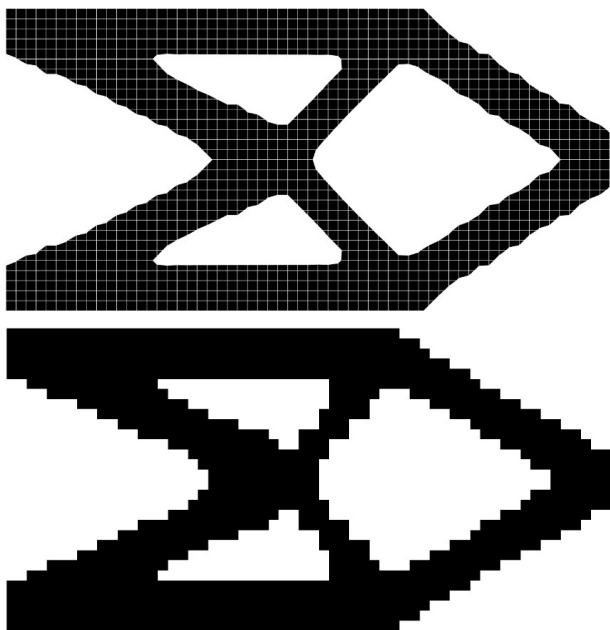


Fig. 4.18. 60×30 Cantilever beam problem proposed method (top) and SIMP method (bottom)

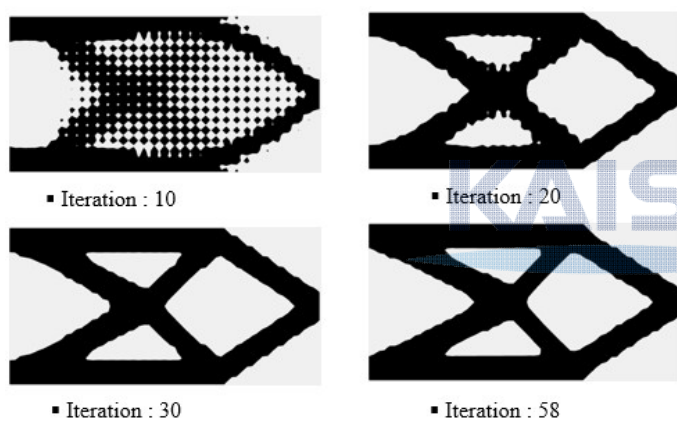


Fig. 4.19. Iterative process of 60×30 elements

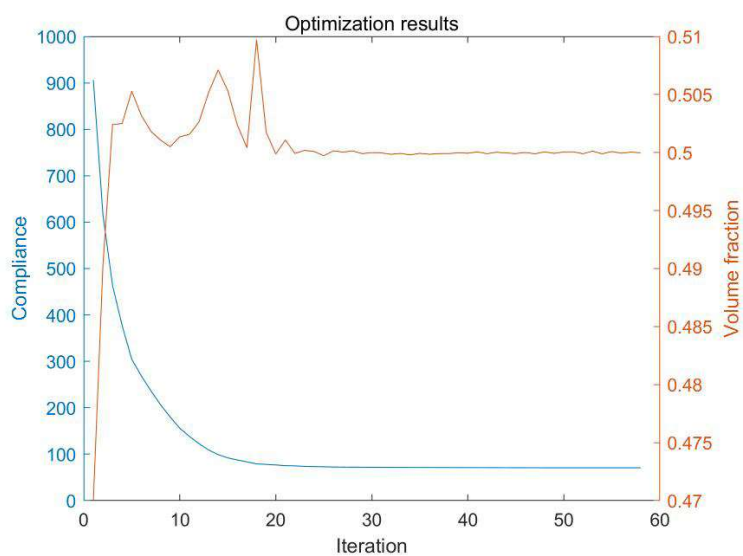


Fig. 4.20. Optimization results for 60×30 elements

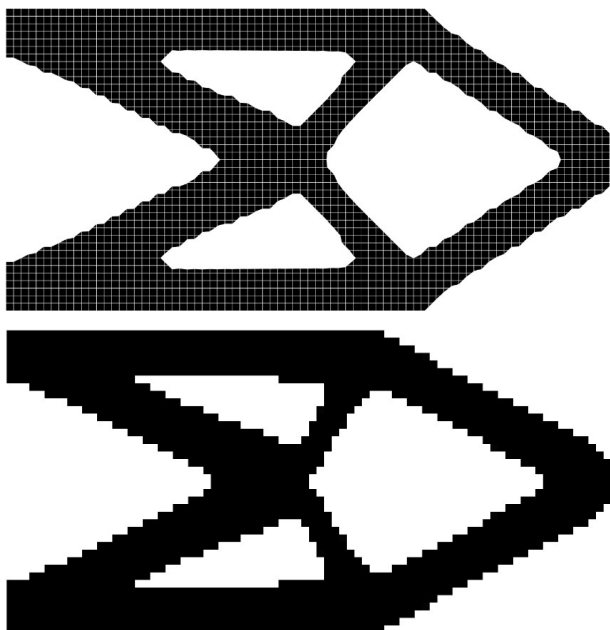


Fig. 4.21. 80×40 Cantilever beam problem proposed method (top) and SIMP method (bottom)

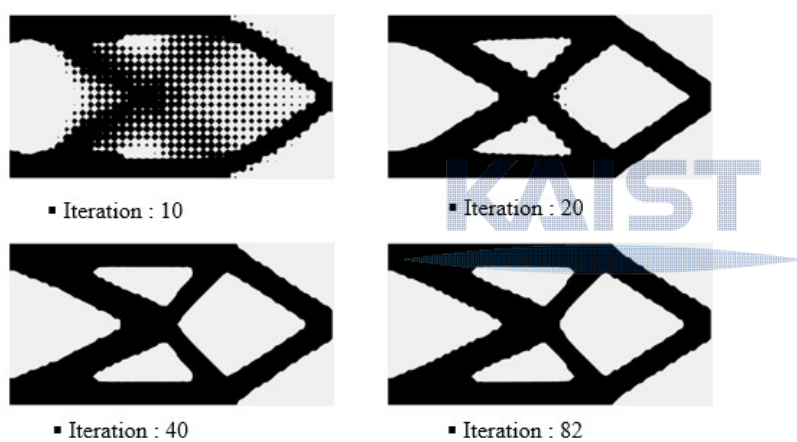


Fig. 4.22. Iterative process of 80×40 elements

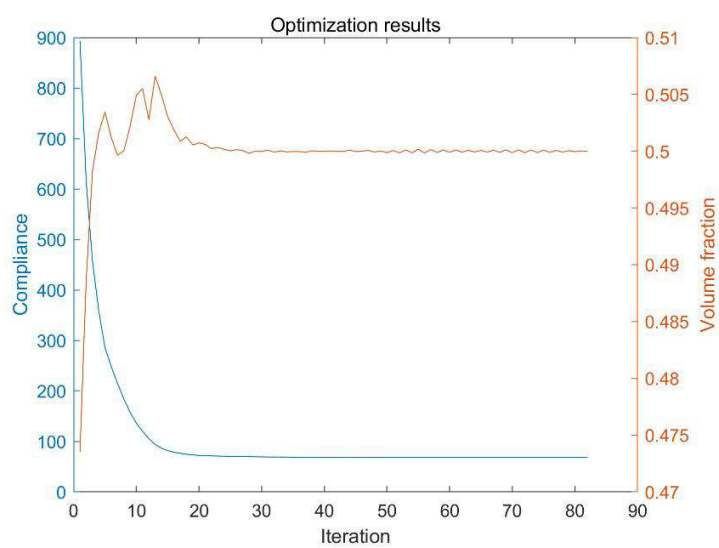


Fig. 4.23. Optimization results for 80×40 elements

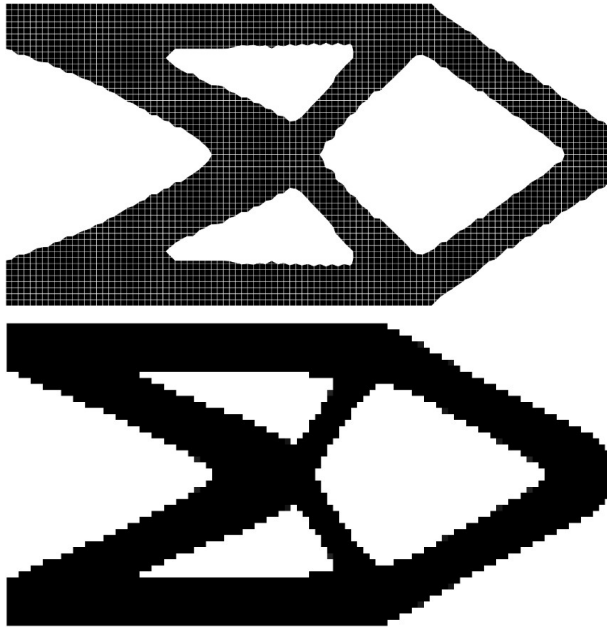


Fig. 4.24. 100×50 Cantilever beam problem proposed method (top) and SIMP method (bottom)

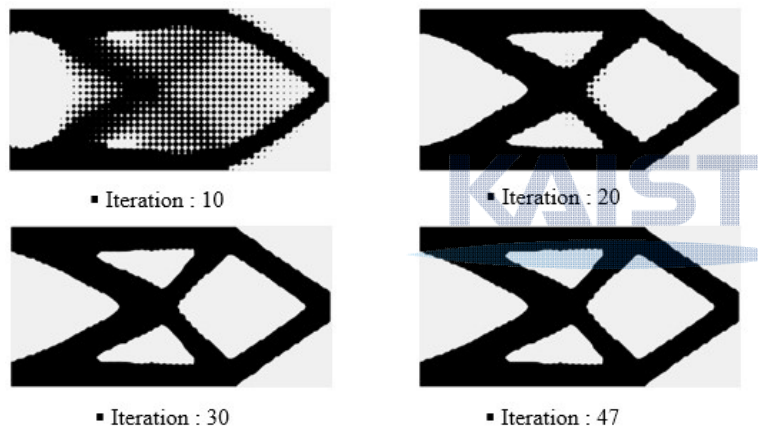


Fig. 4.25. Iterative process of 100×50 elements

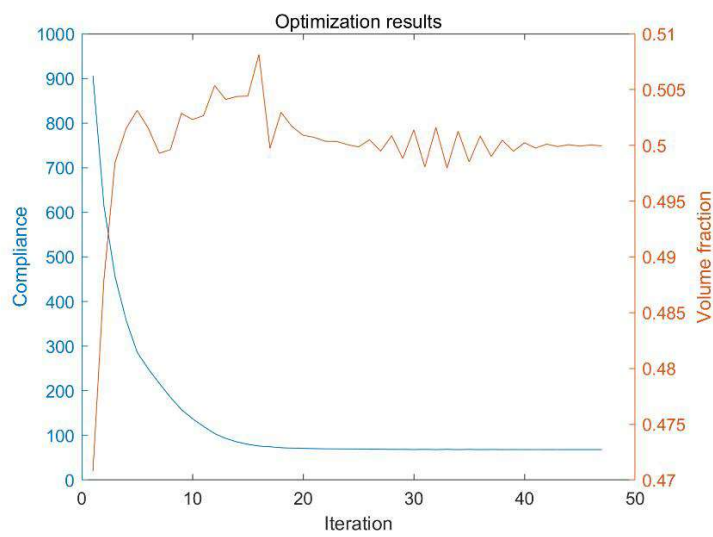


Fig. 4.26. Optimization results for 100×50 elements

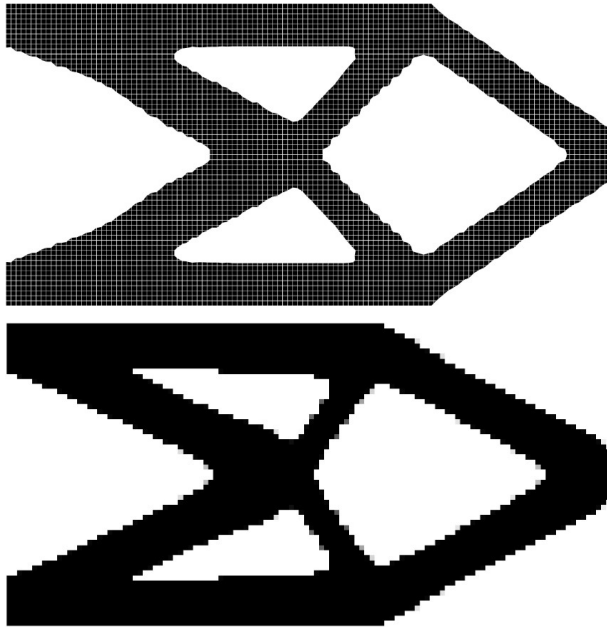


Fig. 4.27. 120×60 Cantilever beam problem proposed method (top) and SIMP method (bottom)

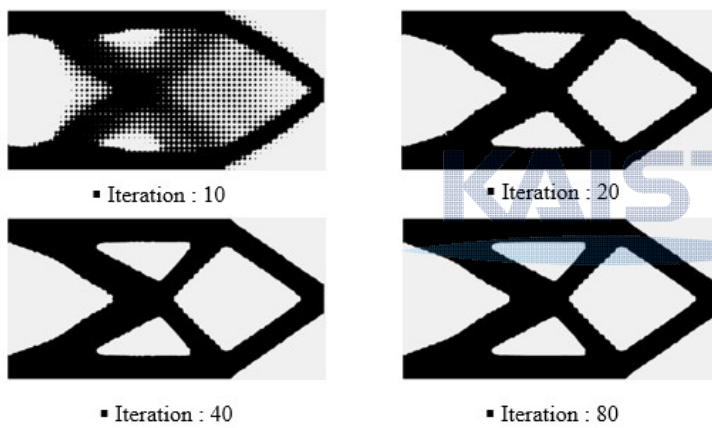


Fig. 4.28. Iterative process of 120×60 elements

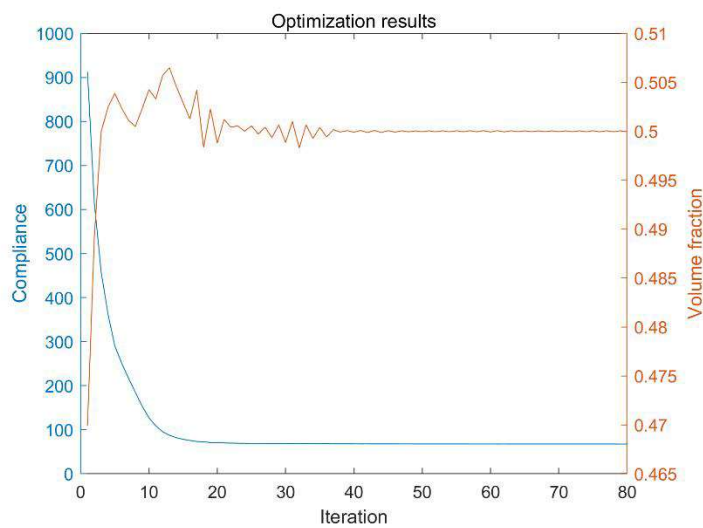


Fig. 4.29. Optimization results for 120×60 elements

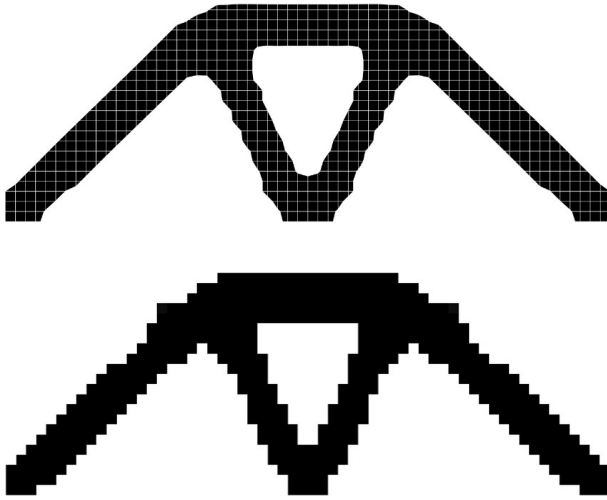


Fig. 4.30. 60×30 Michell type structure problem proposed method (top) and SIMP method (bottom)

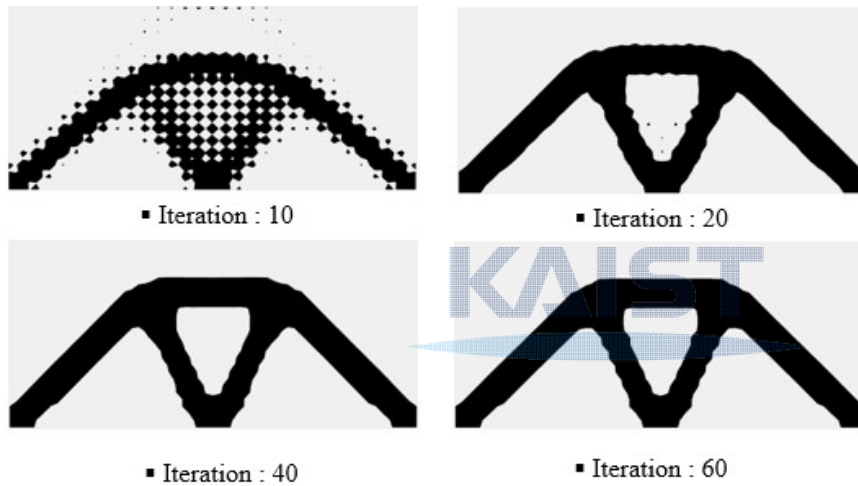


Fig. 4.31. Iterative process of 60×30 elements

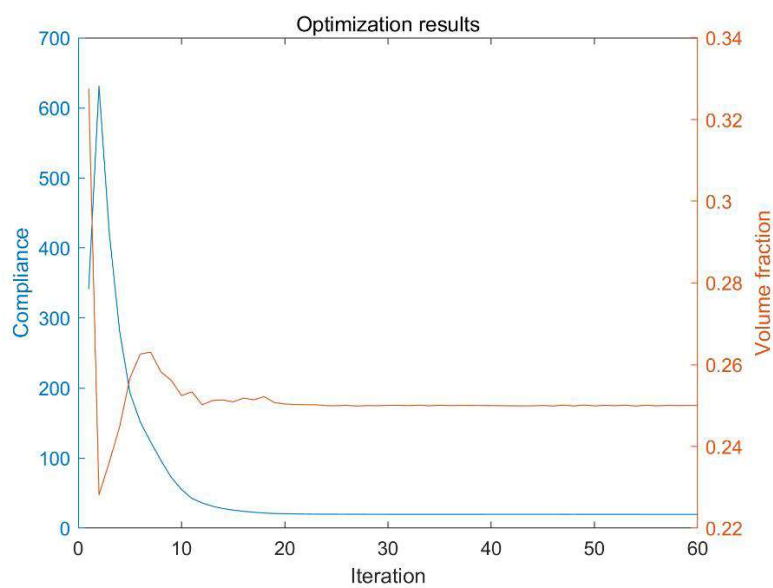


Fig. 4.32. Optimization results for 60×30 elements

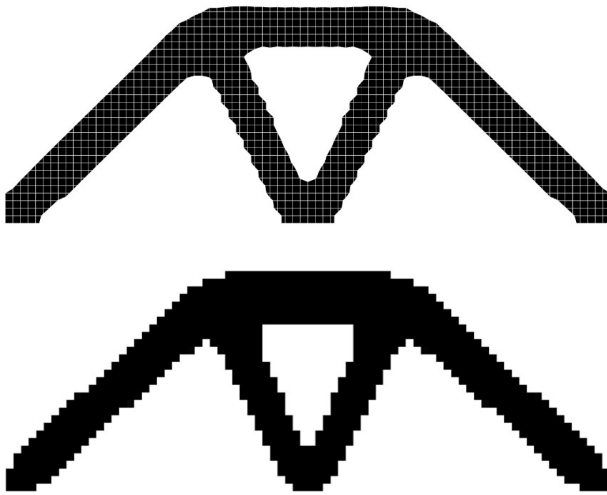


Fig.4.33. 80×40 Michell type structure problem proposed method (top) and SIMP method (bottom)

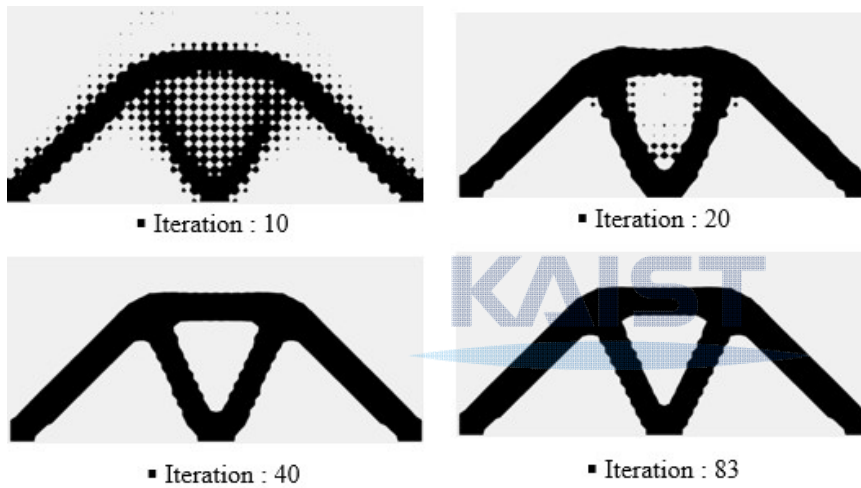


Fig.4.34. Iterative process of 80×40 elements

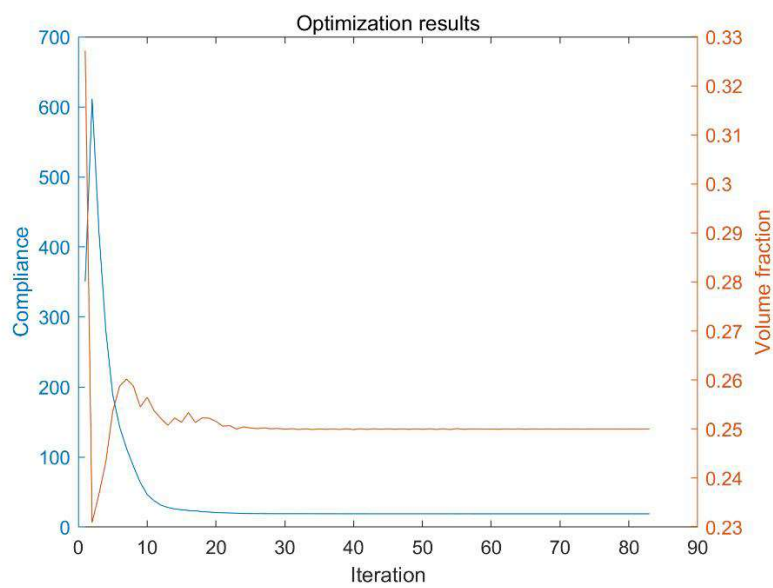


Fig. 4.35. Optimization results for 80×40 elements

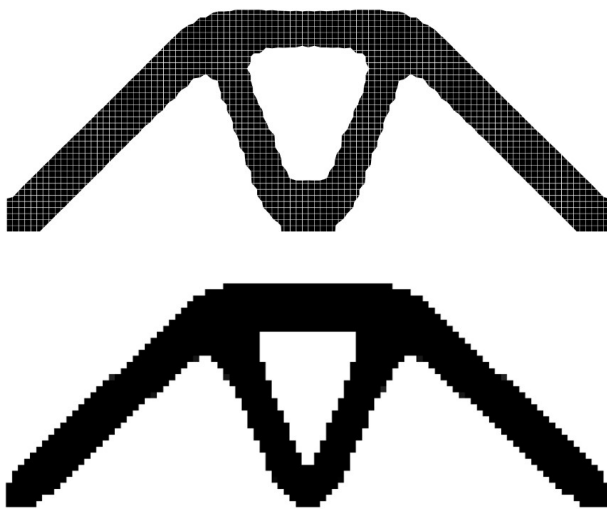


Fig. 4.36. 100×50 Michell type structure problem proposed method (top) and SIMP method (bottom)

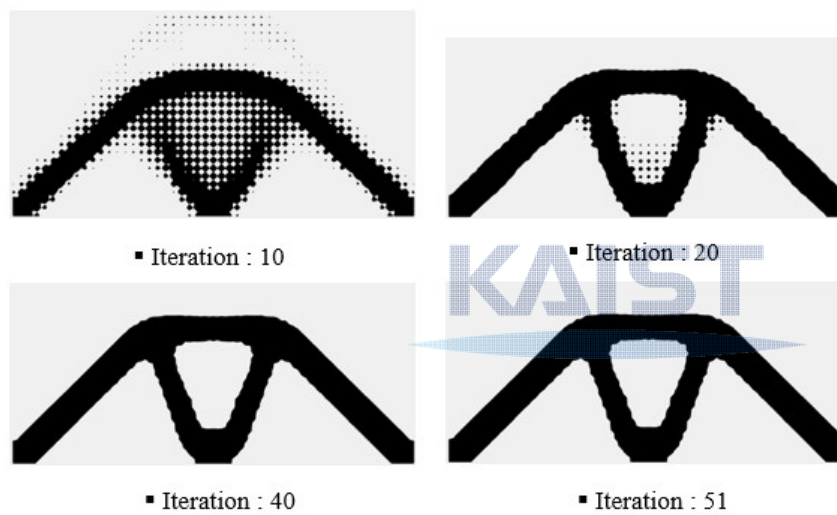


Fig. 4.37. Iterative process of 100×50 elements

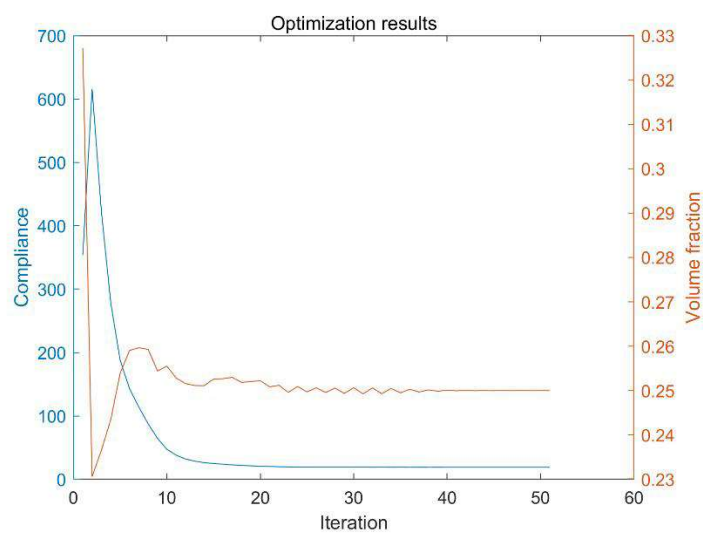


Fig. 4.38. Optimization results for 100×50 elements



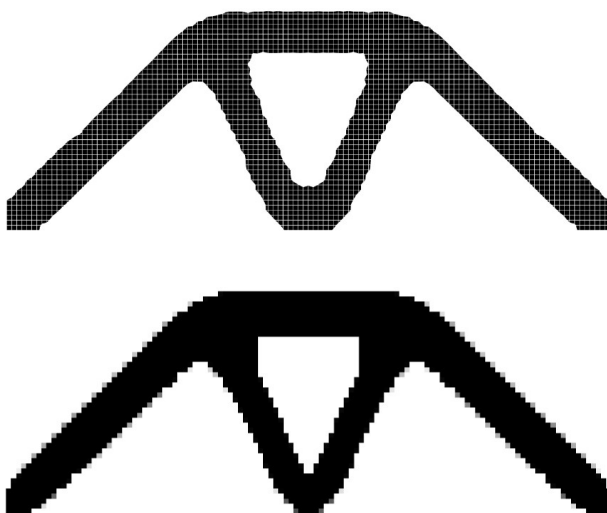


Fig. 4.39. 120×60 Michell type structure problem proposed method (top) and SIMP method (bottom)

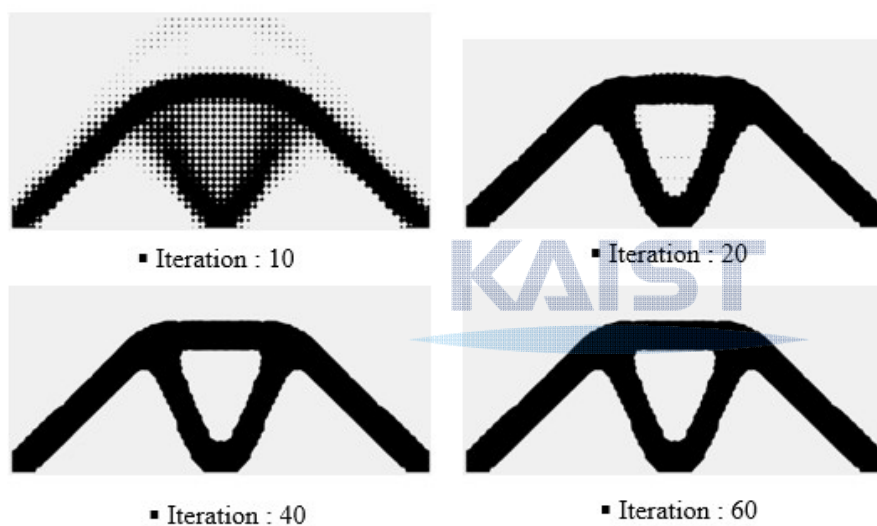


Fig. 4.40. Iterative process of 120×60 elements

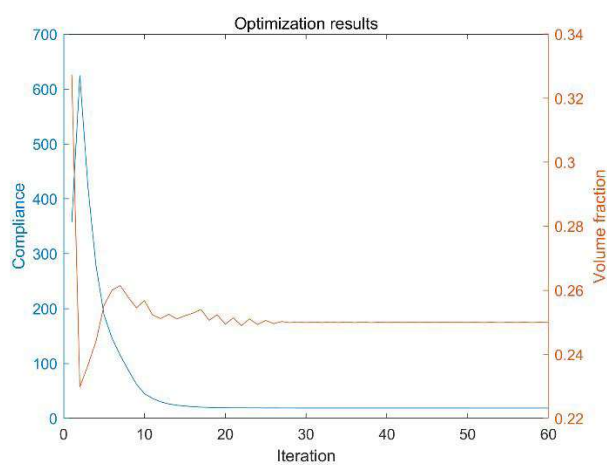


Fig. 4.41. Optimization results for 120×60 elements



## Chapter 5. Conclusions

The purpose of this paper is to obtain continuous boundary of topology optimization results. Element based topology optimization has a limitation in that it has uniform density within an element. This method has the disadvantage of having intermediate density or jagged boundary.

In this study, boundary of optimized design is expressed as iso-density line with nodal density. The stiffness matrix of dividend element by iso-density line was obtained with numerical integration only for solid domain. Main idea of this study is proposal of a new stiffness matrix to avoid numerical instabilities. This makes objective function converge stably in the topology optimization process. The proposed method can obtain clear boundary of optimized design with coarse mesh.

In addition, the proposed method has a more physical meaning than the element-based density method with intermediate density because the proposed method has a binary density 0-1 within elements. It was verified through several numerical examples to get clear boundary.

In the future work, a new modified stiffness matrix equations can be investigate for better performance. This matrix should be proposed to avoid numerical instabilities while minimizing the effect of underestimation of the stiffness due to the penalty factor. Using such a stiffness matrix will have the effect of reducing the gap between physical and nominal compliance.

## Bibliography

- [1] Stainko, Roman. "An adaptive multilevel approach to the minimal compliance problem in topology optimization." *Communications in numerical methods in engineering* 22.2 (2006): 109-118.
- [2] Papalambros, Panos Y., and Mehran Chirchdast. "An integrated environment for structural configuration design." *Journal of Engineering Design* 1.1 (1990): 73-96.
- [3] Nguyen, Tam H., et al. "A computational paradigm for multiresolution topology optimization (MTOP)." *Structural and Multidisciplinary Optimization* 41.4 (2010): 525-539.
- [4] Sethian, James A., and Andreas Wiegmann. "Structural boundary design via level set and immersed interface methods." *Journal of computational physics* 163.2 (2000): 489-528.
- [5] Lee, Dongkyu, Sungsoo Park, and Soomi Shin. "Node-wise topological shape optimum design for structural reinforced modeling of Michell-type concrete deep beams." *Journal of Solid Mechanics and Materials Engineering* 1.9 (2007): 1085-1096.
- [6] Victoria, Mariano, Pascual Martí, and Osvaldo M. Querin. "Topology design of two-dimensional continuum structures using isolines." *Computers & structures* 87.1-2 (2009): 101-109.
- [7] Abdi, Meisam, Ricky Wildman, and Ian Ashcroft. "Evolutionary topology optimization using the extended finite element method and isolines." *Engineering Optimization* 46.5 (2014): 628-647.
- [8] Michell, Anthony George Maldon. "LVIII. The limits of economy of material in frame-structures." *The London, Edinburgh, and Dublin Philosophical Magazine and Journal of Science* 8.47 (1904): 589-597.
- [9] Bendsoe, Martin Philip, and Ole Sigmund. *Topology optimization: theory, methods, and applications*. Springer Science & Business Media, 2013.
- [10] Prager, W., and G. I. N. Rozvany. "Optimal layout of grillages." *Journal of Structural Mechanics* 5.1 (1977): 1-18.
- [11] Bendsoe, Martin Philip, and Noboru Kikuchi. "Generating optimal topologies in structural design using a homogenization method." (1988).
- [12] Bendsoe, Martin P. "Optimal shape design as a material distribution problem." *Structural optimization* 1.4 (1989): 193-202.
- [13] Bendsoe, Martin P., and Ole Sigmund. "Material interpolation schemes in topology optimization." *Archive of applied mechanics* 69.9-10 (1999): 635-654.
- [14] Xie, Y. M., and Grant P. Steven. "Optimal design of multiple load case structures using an evolutionary procedure." *Engineering computations* (1994).
- [15] Yang, X. Y., et al. "Bidirectional evolutionary method for stiffness optimization." *AIAA journal* 37.11 (1999): 1483-1488.
- [16] Sigmund, Ole. "On the design of compliant mechanisms using topology optimization." *Journal of Structural Mechanics* 25.4 (1997): 493-524.
- [17] Rojas-Labanda, Susana, and Mathias Stolpe. "Benchmarking optimization solvers for structural topology optimization." *Structural and Multidisciplinary Optimization* 52.3 (2015): 527-547.
- [18] Bendsoe, Martin P., and Ole Sigmund. *Optimization of structural topology, shape, and material*. Vol. 414.

Berlin: Springer, 1995.

- [19] Svanberg, Krister. "The method of moving asymptotes—a new method for structural optimization." *International journal for numerical methods in engineering* 24.2 (1987): 359-373
- [20] Sigmund, Ole. Design of material structures using topology optimization. Diss. Technical University of Denmark, 1994.
- [21] Bruns, Tyler E., and Daniel A. Tortorelli. "Topology optimization of non-linear elastic structures and compliant mechanisms." *Computer methods in applied mechanics and engineering* 190.26-27 (2001): 3443-3459.
- [22] Bourdin, Blaise. "Filters in topology optimization." *International journal for numerical methods in engineering* 50.9 (2001): 2143-2158.
- [23] Guest, James K., Jean H. Prévost, and Ted Belytschko. "Achieving minimum length scale in topology optimization using nodal design variables and projection functions." *International journal for numerical methods in engineering* 61.2 (2004): 238-254.
- [24] Borrvall, Thomas, and Joakim Petersson. "Topology optimization using regularized intermediate density control." *Computer Methods in Applied Mechanics and Engineering* 190.37-38 (2001): 4911-4928.
- [25] Lorensen, William E., and Harvey E. Cline. "Marching cubes: A high resolution 3D surface construction algorithm." *ACM siggraph computer graphics* 21.4 (1987): 163-169.
- [27] Sukumar, Natarajan, et al. "Modeling holes and inclusions by level sets in the extended finite-element method." *Computer methods in applied mechanics and engineering* 190.46-47 (2001): 6183-6200.
- [28] Lee, Kang-Heon, and Phill-Seung Lee. "Nonlinear hydrostatic analysis of flexible floating structures." *Applied Ocean Research* 59 (2016): 165-182.
- [29] Sigmund, Ole. "Morphology-based black and white filters for topology optimization." *Structural and Multidisciplinary Optimization* 33.4-5 (2007): 401-424.